

Invited research article

Using Structure from Motion photogrammetry to assess large wood (LW) accumulations in the field

Gabriel Spreitzer ^a*, Jon Tunnicliffe, Heide Friedrich

^a Department of Civil & Environmental Engineering, University of Auckland, Auckland, New Zealand

^b School of Environment, University of Auckland, Auckland, New Zealand

^c Department of Civil & Environmental Engineering, University of Auckland, Auckland, New Zealand

ARTICLE INFO

Article history:

Received 9 December 2018

Received in revised form 20 August 2019

Accepted 21 August 2019

Available online 26 August 2019

Keywords:

Large Wood (LW) accumulation

Volume evaluation

Structure from Motion (SfM)

Smartphone SfM in-situ

ABSTRACT

River systems in forested catchments are strongly influenced by wood and sediment loading from both natural (e.g. mass wasting) and anthropogenic (forestry) sources. In order to effectively manage impacts on property, infrastructure and the broader ecosystem, as well as to better assess the interactions between large wood (LW), channel morphology and flow hydraulics, more efficient and accurate surveying techniques are required. We present an evaluation of Structure from Motion (SfM) photogrammetry and point-cloud-based techniques for capturing the geometry and volume of LW in the field. Wood accumulations can be notoriously complex 3D objects, with multi-scalar features, and thus difficult to quantify with photogrammetric methods. We introduce a novel workflow to generate volumetric information of organic material accumulations, using SfM and a suite of meshing algorithms. The volumes of two accumulations are assessed individually, using several meshing techniques, and are compared with more conventional volume estimates. Results show volumetric variations of <19% between the interpolated volumes from point clouds and those of meshes, and a slight overestimation of volumes using simple geometric primitives. We discuss the nature of noise and errors that arise within processed results from SfM software (Pix4D) and offer some criteria for generating high quality point cloud models of highly irregular and complex organic material piles. More detailed 3D mesh representations of LW accumulations will be effective for improving computer-aided modelling of jam-induced floods, backwater effects and impacts on channel morphology. Measuring the size and geometric distributions of wood elements, assessing deposit volume and porosity, or estimating the proportion of organic fine material in the deposit, are important quantities to be assessed for wood accumulations in rivers. The photogrammetric methodology presented herewith will be useful for forestry and freshwater managers to estimate LW quantities, but also to develop accurate 3D models of prototype LW accumulations, independent of camera model and environmental condition, for a range of applications and LW accumulation assessment.

© 2019 Elsevier B.V. All rights reserved.

1. Introduction

1.1. Large wood (LW)

Natural forest disturbance and modern forest harvesting techniques produce significant quantities of large wood (LW) in steep mountain terrain. Once recruited to the fluvial system, this organic material tends to accumulate and develop into jams. LW is defined according to the characteristic dimensions (i.e. diameter) of the pieces. A widely used criteria is wood pieces with a minimum diameter of 0.1 m and at least 1 m length (Nakamura and Swanson, 1994; Jackson and Sturm, 2002; Baillie et al., 2008; Wohl and Jaeger, 2009; Ravazzolo et al.,

2015; Mao et al., 2017). Gurnell (2013) defined a LW accumulation as a deposit consisting of several wood pieces, while at least one wood piece shows LW dimensions and blocks a stream section partly or fully.

LW is, in general, a valuable part of a fluvial ecosystem, providing habitat and environmental complexity for numerous living organisms (Fausch and Northcote, 1992). Wood can protect stream sections from erosion and it regulates a river's sediment budget, due to sediment storage and energy dissipation processes (Megahan and Nowlin, 1976; Swanson et al., 1976; Platts et al., 1983; Bilby and Ward, 1989; Montgomery et al., 2003). Besides the beneficial ecological and hydraulic roles of LW in fluvial systems, there are also challenges. The presence of LW accumulations in river channels may dramatically increase the risk potential for human population and infrastructure during high-flow events (Braudrick and Grant, 2001; Le Lay et al., 2013; Schmocker and Weitbrecht, 2013). Clogging processes at constricted cross-sections can result in a reduction of the conveyance capacity

* Corresponding author.

E-mail addresses: gspr390@aucklanduni.ac.nz (G. Spreitzer), j.tunnicliffe@auckland.ac.nz (J. Tunnicliffe), h.friedrich@auckland.ac.nz (H. Friedrich).

(Rusyda et al., 2014; Gschnitzer et al., 2017), leading to overtopping of stop banks and flooding of the riparian zone, as well as changes in channel morphology (local erosion and aggradation processes), and backwater effects (Knauss, 1995; Le Lay et al., 2013). Backwater effects potentially increase static and hydrostatic pressure conditions at the blocked location, accompanied by stress on adjacent hydraulic structures and the environment. Organic fine material (OFM) can fill interstitial space within the LW jam, decreasing the porosity of the deposit and further reducing the effective cross-sectional area. OFM is defined as discrete wood pieces, leaves or grass with smaller dimensions than LW, and a minimum size of 1 mm. This added complexity within the jam leads to further accumulation and exacerbation of backwater effects (Schmocker and Weitbrecht, 2013; Schalko et al., 2016). The role of OFM in jams and flood dynamics has largely been neglected in past research, however it is assumed to significantly affect hydraulic flow behaviour and LW accumulation structure.

There are a number of important quantities to be assessed in inventorying, monitoring and modelling LW accumulations: deposit geometry (Piegay, 1993), accumulation porosity (addressed by Boivin and Buffin-Bélanger (2010)), orientation of wood components (Ruiz-Villanueva et al., 2016), but also obtaining accurate measurements of the bulk volume of the deposit with regards to the influenced stream reach, which all affect flow hydraulics and channel morphology significantly (Gippel, 1995; Gschnitzer et al., 2017; Schalko et al., 2018). In previous studies, several methods have been applied to estimate LW volume in riparian zones and stream channels as a review of Ruiz-Villanueva et al. (2016) reveals. For LW accumulation assessment and wood-budgeting, Boivin et al. (2015) considered measurements of the 'air-wood' volume by applying a rectangular model with accumulation length, width and average height. Other volume assessing methods include developing scaling relationships relating wood accumulation to catchment size, the proportion of forest cover in the catchment upstream, forested river length (Uchiogi et al., 1996), and the density of landslide occurrence upstream (Rigon et al., 2008). Wood load has further been related to wood flux estimations, the nature of terrestrial supply sources, decay rates, and riparian storage (Benda and Sias, 2003). Other researchers, such as Cordova et al. (2006), Brown et al. (2014) and Dixon and Sear (2014), counted and measured single wood logs along river sections in order to get a more accurate estimation of LW volume. None of the previous studies have considered irregularities of wood logs, which impacts the accuracy of estimates of volume and porosity. LW volume can be determined accurately using water displacement methodology (Brown et al., 2014), however this method is not efficient for estimates of larger wood quantities, e.g. an entire LW accumulation and whole stream sections. Although volumetric assessment of LW has been addressed throughout various LW investigations (Harmon et al., 1986; Lienkaemper and Swanson, 1987; Gurnell et al., 2002; Webb and Erskine, 2003; Manners and Doyle, 2008; Dixon and Sear, 2014; Wohl et al., 2017; Martin et al., 2018), the stated volumes are mostly rough estimates rather than exact measurements. The importance of obtaining precise assessments varies with the working scale of the study; rough measures are fine for broader inventories of LW deposition and wood-flux budgeting, but site-specific process studies may require more refined estimates. The complexity of these deposits introduces some important challenges for accurately resolving volumes quickly, with minimum field effort.

Managers and researchers are often interested in capturing the volume of the LW accumulations, as well as the composition, including sediments, OFM and LW pieces. High-resolution photogrammetry can therefore be used for (i) LW budgeting, in order to estimate how much organic material has been mobilized and deposited following higher magnitude floods, (ii) identification of key logs, for a better understanding of initial LW accumulation mechanisms and deposition processes, (iii) monitoring existing LW accumulation at

constricted cross-sections, to observe how wood structures develop over time, and (iv) estimation of backwater effects that arise during flood events, due to the reduced cross-sectional flow area.

1.2. High-resolution techniques for LW estimation

Quantitative assessment of fluxes of wood and sediment through river systems is undergoing something of a revolution, with the introduction of light detection and ranging (LiDAR) scans (Geerling et al., 2007; McKean et al., 2014; Magnussen et al., 2018), and Structure from Motion (SfM) acquisition for capturing the geometric configuration of depositional forms (Hildreth et al., 1995; Westoby et al., 2012; Javernick et al., 2014; Prosdociami et al., 2015; Smith et al., 2016; Wróżyński et al., 2017; Tunncliffe et al., 2018). This has important implications for wood budgeting applications (Janisch, 2006; Steeb et al., 2017), where quantitative differences between river channel configuration can be used to assess system trajectories and rates of transport. Floodplains, bars, and woody accumulations can be captured at a density of over a million points/m² (Smith et al., 2016).

Advanced measurement technology and methodologies have shed further light upon the dynamics of LW accumulations. Airborne remote sensing methodologies have been used to quantify volumes of large wood accumulations for mass balance models (Steeb et al., 2017), detection of instream LW (Atha and Dietrich, 2016), and identification of LW sources (Kasprak et al., 2012), however such studies tend to capture only coarse geometry of LW with a resolution of 1–8 points/m² interpolated from LiDAR scans. This resolution is sparse, relative to wood size (Fig. 1), and there is little potential for extracting detailed information about surface texture and volume, leading to the need for further manual quantification methods (Richardson and Moskal, 2016). Some studies have used terrestrial laser scanning (TLS) for LW surveying (Boivin and Buffin-Bélanger, 2010; Tonon et al., 2014; Grigillo et al., 2015) and have achieved spatial resolutions in the range of 150 points/m² to 1 point/mm² and higher. Other LW researchers, using conventional photogrammetry techniques, have reported inaccuracies when wood pieces were smaller than individual pixels (Marcus et al., 2003). With lower resolution imagery, it can also be challenging to distinguish LW from gravel and other objects with similar spectral characteristics (Colvard, 1998; Wright et al., 2000).

SfM photogrammetry is becoming a powerful tool to map surfaces and model topographic terrains (Morgan et al., 2016; Smith et al., 2016). In-situ digital photogrammetry has already been proven effective in fluvial geomorphology studies, from aerial mapping of larger stream sections (Immerzeel et al., 2014; Dietrich, 2016; Tunncliffe et al., 2018) to close-range studies of grain sizes characteristics, in a range of a few millimeters (Snapir et al., 2014; Ferreira et al., 2017; Wróżyński et al., 2017). The use of smartphones for SfM photogrammetry in the field has been demonstrated by Nocerino et al. (2017), working on a 3D acquisition tool for mobile-based object reconstruction, and Micheletti et al. (2015b), who developed a digital terrain model (DTM) from a 5MP smartphone camera. Even with relatively low-resolution images, suitable 3D models can be generated. The level of detail captured by lower resolution cameras can be increased with a larger number of images (Dikovski et al., 2014) and close-range image acquisition. In SfM photogrammetry applications, prototype equivalent pixel size varies in a range of $\approx 10^2$ to 10^3 points/m² (Smith and Vericat, 2015).

Only a few applications using SfM (exclusively) for LW research have been documented (Byrnes and Hasbargen, 2016; Truksa et al., 2017; Sanhueza et al., 2018; Sanhueza et al., 2019). In general, it has been found that SfM photogrammetry shows similar performance to TLS and aerial laser scans (ALS) in overall model quality (Mancini et al., 2013; Kaiser et al., 2014; Tonon et al., 2014), however, it outperforms substantially when it comes to time efficiency and operation costs. The Skagit Watershed Council (2017) described in their report that it is generally possible to estimate volumes of LW accumulations

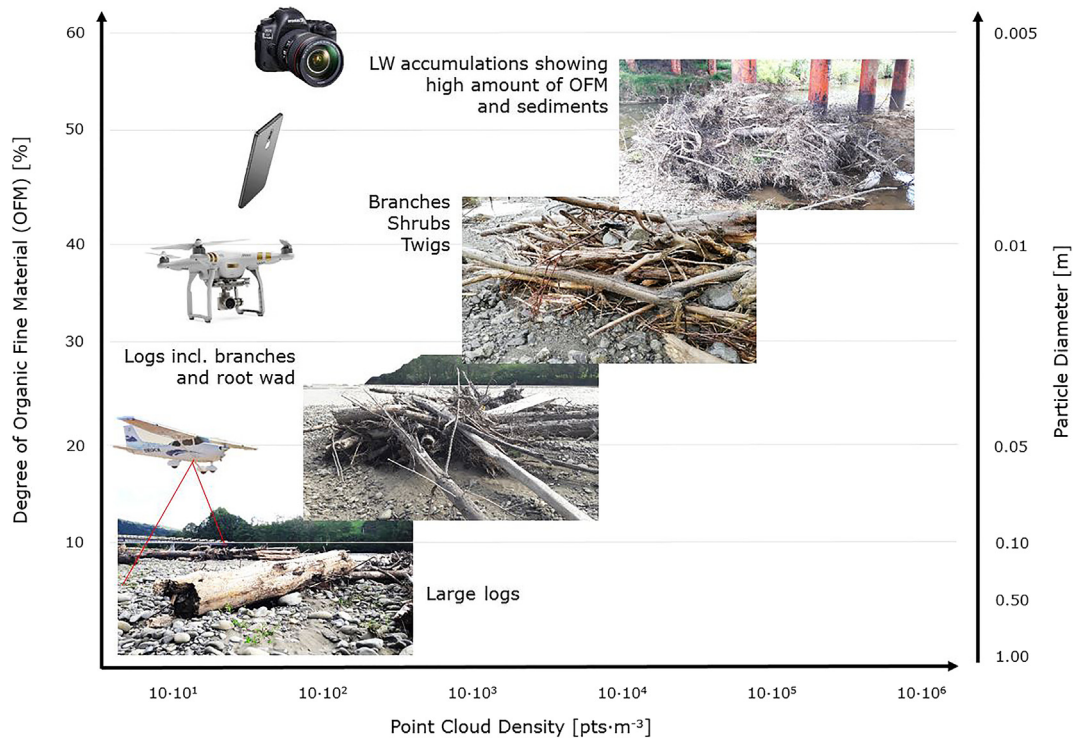


Fig. 1. LW composition and required points/m³ to resolve a SfM photogrammetry point cloud model.

using SfM photogrammetry, albeit with a few difficulties obtaining consistent results under field conditions.

A hybrid approach was used in the course of the Trinity River Restoration Program (TRRP, 2018), where LW jams were investigated using both TLS and SfM photogrammetry. A comparison of these point cloud models showed that TLS provides a higher overall point density, however SfM generates better surface models because of more viewing angles (Peterson et al., 2015). Peterson et al. (2015) indicated that half of the computed SfM photogrammetry tie points got lost because of water reflections and background vegetation. SfM photogrammetry for LW accumulations is thus limited to reconstructing features above the water surface, and the method cannot generate high quality point clouds when water is moving, due to a lack of matching points in the images. Two general principles underlie successful SfM applications: (i) the object and surroundings in the images should be stationary, and (ii) when using low quality images, the number of images should be increased to maintain overall quality of the generated point clouds (Dikovski et al., 2014).

1.3. Unstructured point cloud mesh

In parallel with developments in photogrammetry and active scanning techniques, the mathematical techniques for interpolating volume from noisy scattered 3D point cloud data (point set processing) have been advancing, as outlined in the work of Berger et al. (2017). In geographical and land-management applications, LiDAR and photogrammetry point clouds are commonly interpolated into a 2D raster format, using weighted triangulation (e.g. inverse distance weighted (IDW), nearest neighbour) or binned averaging of point elevations. Resolving finely-featured, complex, unordered 3D surfaces is more challenging. The pathway from an unordered point cloud to a stand-alone 3D object with 'watertight' surfaces (no holes in the enclosing mesh) is fraught with a number of difficulties, and each meshing technique has strengths and weaknesses, depending on the application.

The challenge of generating a mesh from an unstructured point cloud is a rapidly evolving frontier in computational geometry and

computer graphics (Fuchs et al., 1977; Marton et al., 2009; Kazhdan and Hoppe, 2013). The development of meshes, voxels (volumetric pixels) and other digital representations of physical structures from unstructured point clouds has flourished in the medical sciences (Palagyi et al., 2006; Mattingly et al., 2015), archaeology (Doneus et al., 2011; Brutto and Meli, 2012), agriculture and forestry (Rosell et al., 2009; Wallace et al., 2016), computer-aided design (Kim and Li, 2006; Liu et al., 2014; Peterson et al., 2015; Shepherd and Treddinick, 2015) and many other natural sciences. Assessment of tree canopy (Riley and Crowe, 2006) and stem volumes (Dassot et al., 2012; Hosoi et al., 2013; Zhang et al., 2017) has been a strong motivation for converting complex point clouds into volumetric mesh.

Software and programming libraries for meshing arbitrary point clouds, such as the Computational Geometry Algorithms Library (CGAL, 2018), CloudCompare (CloudCompareV2, 2016), MeshLab (Cignoni et al., 2008), OpenMesh (www.openmesh.com), and Point Cloud Library (PCL) by Rusu and Cousins (2011), available as open-source mesh processing tools, have rendered many of these techniques more accessible to general users.

1.3.1. Cleaning

The quality of the details captured within the volumetric model will depend greatly on the resolution of the SfM model relative to the scales of interest (Fig. 1), as well as noise from interpolation errors and the bundle adjustment (BA) process. Dense point clouds are required for good surface reconstruction (Maiti and Chakravarty, 2016), although there are gains to be made by cleaning and subsampling point clouds for more uniform distribution and better data processing performance (Pauly et al., 2002; Cheng and Lau, 2017). Point clouds exceeding roughly ten million points become difficult to manage on current processors (e.g. multi-core Intel i7, AMD Zen series) with 32Gb + of RAM. Thus, it is worth giving some consideration to the required resolution for the survey study area. Point cloud software will have numerous options for segmenting or down-sampling the point cloud; points can be selected at random, or bias can be used to selectively thin points



Fig. 2. Whakatawai River with scour hole and LW accumulation (a), single emerging wood logs as part of the buried accumulation structure (b), fine gravel bar development in downstream direction and coarse gravel bar development upstream (c) in October 2017 when SfM data have been obtained, in comparison to a further accumulation stage in March 2018 (d).

within clusters, balancing the overall point density within the subsampled cloud.

1.3.2. Normal estimation

Meshing of point clouds requires orientation information - normals - of individual points for realistic surface reconstruction: the raw input points have no inherent structure or orientation information. This orientation information for points can be computed with consideration of neighbouring points and view directions. There are several strategies for estimating the outward-facing direction for points that locally define a surface (Mitra and Nguyen, 2003; Rusu, 2009). A larger number of images may additionally contribute to improved model accuracy, by enabling the generation of denser meshes (Micheletti et al., 2015b).

1.3.3. Surface reconstruction

In contrast to sedimentary surfaces, such as floodplains and bars, fibrous targets, such as organic materials, present a number of challenges for volumetric capture, because of the highly complex and multi-scalar nature of the constitutional elements - from fine organic detritus, to large logs, to stems and branches with intricate, involuted and interwoven details (Fig. 1). A large variety of surface meshing algorithms is available (Berger et al., 2014), however, the most common ones are

Delaunay-based methods (Cazals and Giesen, 2006), and screened Poisson surface reconstruction (PSR) (Kazhdan et al., 2006), as the codes are highly stable and reliable (Berger et al., 2014).

1.4. Objectives

Methodological limitations restrict current understanding of LW dynamics (Thevenet et al., 1998; Peterson et al., 2015; Steeb et al., 2017). In this paper we focus specifically on the potential of SfM photogrammetry as a technique for assessing LW accumulation volume. The detailed photogrammetric point clouds (point density $> 10^6 \text{ m}^{-2}$) generated from photos taken at two study sites yield accurate volumetric information of wood accumulations, with a range of possible applications independent of camera model and environmental conditions.

The objectives of this paper are to:

1. Evaluate quantitative LW accumulation measurements from the field and outline special considerations for capturing the geometry of complex LW accumulations.
2. Evaluate techniques that represent LW accumulation surfaces, from geometric primitives to Delaunay triangulation, to implicit meshing techniques, such as PSR.

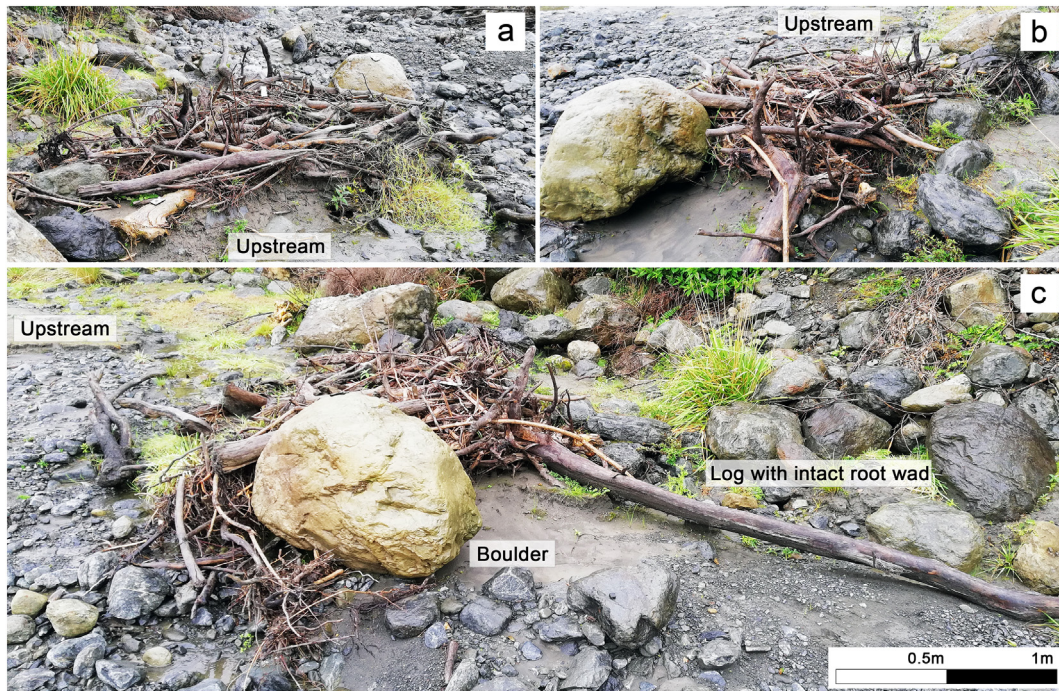


Fig. 3. Organic material accumulation at the Hapuku River. Downstream view (a), upstream view (b) and a perspective showing the boulder and wood log with intact root wad, initiating the accumulation (c).

3. Assess LW accumulation volume, using a software aided '2.5D' parallel-lepipiped approach, between a lower bounding surface and the SfM model.

We further discuss practical applications and prospective directions of further analysis, including classification of the point cloud, bulk properties (porosity, density) and assessing fines content. The generated point cloud and mesh models may provide key information on LW accumulation structure (geometry) and surface texture that can be useful for future processing and the application in computer-aided modelling.

2. Study sites

2.1. Whakatiwai River – Hunua Ranges, North Island, New Zealand

The Whakatiwai River is a 4th order stream located in the North Island of New Zealand (Fig. 4) (MFE, 2010). The stream is characterized by a relatively short distance of 10 km from source to estuary, draining a catchment area of roughly 12 km², with a maximum elevation of about 500 m above sea level (m.a.s.l.). Land cover was estimated to be roughly 50% forests in the upper catchment and 50% grassland in the lower regions (Jones, 2017). At the Whakatiwai bridge (37°05'14.2"S;

175°18'05.5"E), shortly upstream the estuary into the Firth of Thames, an organic material accumulation was observed at the central pier column (Fig. 2a). The accumulation shows signs of upstream gravel bar development, with some accompanying scour (Abbe and Montgomery, 1996; Abbe and Montgomery et al., 2003). The wetted channel width at the bridge cross-section is 15 m, with signs suggesting a bankfull width of about 25 m (lower edge of bridge deck). The height of the organic material accumulation was measured to be 1.1 m above water level. Left and right wings of the accumulation extended 2 to 2.6 m, measured from the pier centre. The consolidated accumulation shows a wide base, narrowing toward the top. Field photos of the LW accumulation (Fig. 2 and Fig. 4) document the accumulation composition. The organic material accumulation at the Whakatiwai River comprises roughly 10% LW and another 10% of branches and wood particles with a diameter in a range of 0.02 to 0.10 m. OFM occupies about 55% of the entire accumulation. The remaining 25% consists of gravel, sand and silt, in a mixture with organic particles.

2.2. Hapuku River – Kaikōura, South Island, New Zealand

The catchment area of the Hapuku River is located in the Kaikōura Ranges (Fig. 4), with peaks of 2.600 m.a.s.l. (Mount Manakau). The

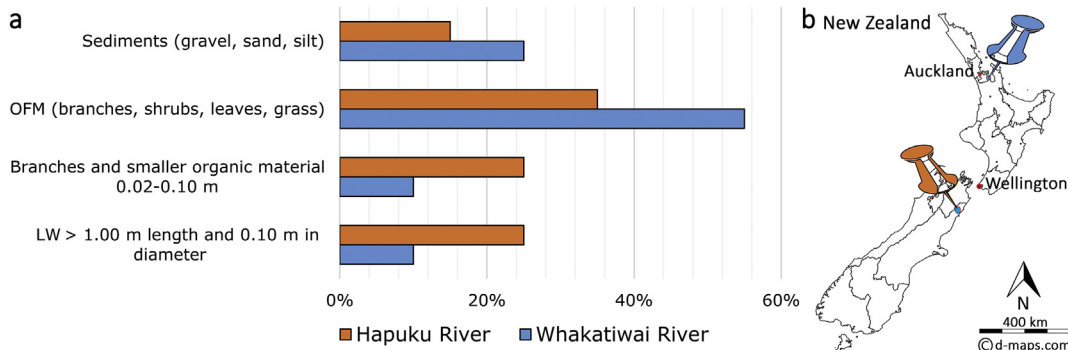


Fig. 4. Compositional estimates of the accumulation at the Whakatiwai River and the Hapuku River sites.

Hapuku River runs a relatively short distance (20 km) from the alpine to the South Pacific Ocean, north of the town of Kaikōura. The Hapuku River is a 5th order stream with one main tributary, the Puhī Puhī River (MfE, 2010). The catchment area is 135 km², covered mainly (55%) by indigenous vegetation, 25% naturally bare, 19% grassland and only 1% exotic forest (Jones, 2017). The channel bed shows large amounts of indigenous wooden particles, with a broad variety of tree species. The lower reaches the Hapuku River braid into multiple channels. An organic material accumulation as shown in Fig. 3, was identified in the Hapuku stream channel (42°18'0.24"S; 173°41'31.2"E) at an elevation of 168 m.a.s.l. The channel spans 15 m, with a few intervening vegetated channel bars at the observed cross-section. A boulder (1 × 0.9 × 0.6 m, a-b-c axis), together with a log (4 m long and 0.17 m in diameter), provided an anchor point for the retention of organic material (Fig. 3c). The log aligns with the flow direction and shows an intact root wad facing upstream. Immediately upstream of the root wad, woody material was clogged to an average height of 0.40 m. The Hapuku accumulation shows a higher number of LW components, which was visually estimated to be 25% in the field (Fig. 4). The accumulation contains just under 60% of OFM, resulting in 85% organic material for the entire accumulation, whereas the remaining 15% are considered to be abiotic fine material (sediments).

3. Methodology

3.1. Camera models

To promote optimum overlap (matches) for high quality digital elevation model (DEM) reconstruction (Gruen, 2012), our data sets comprised 72 and 120 oblique images obtained with two standard camera devices, (i) two GoPro Hero3 Black Edition cameras with a 12MP sensor and (ii) a 16 + 2MP Huawei Nova 2i smartphone camera.

The Whakatiwai River dataset was obtained using GoPro cameras (Table 1). Two GoPro cameras were installed on a portable aluminium stand. The cameras were set 0.4 m apart with converging fields of view, set 20° toward the centre. The cameras were controlled via tablet to capture images simultaneously. Altogether 36 images of the organic material accumulation were taken with each camera, resulting in a dataset of 72 close-range images. Eight cylindrical rulers, each 200 mm long, were placed on and around the accumulation for scaling purposes. Parts of the stream channel were covered by water, which obscured views of a small section of the organic material accumulation. The sky was slightly overcast on the day of image acquisition, ensuring very good light conditions.

The Hapuku River dataset was obtained with a standard smartphone device, a Huawei Nova 2i (Table 1). This relatively inexpensive smartphone has two rear cameras, 16MP and a secondary 2 MP, to add further depth information to the images. Images from the two cameras are integrated directly on the smartphone. To scale the jam formation, four checker boards, 100 to 200 mm long and 50 mm wide, with 25 mm squares, were placed in the area of the organic material accumulation. The area of interest was roughly 20 m² in size, and photos were taken from a distance of 1 to 3 m from the surface of the accumulation. Images in the Hapuku stream channel were obtained during very low runoff conditions. No water surfaces were captured in any of the images. Weather conditions were strongly overcast with diffuse light conditions, providing good conditions for field SfM photogrammetry.

3.2. Image acquisition

The dataset contains oblique images taken from positions at ground elevation to ~2 m above ground. We aimed to capture as much surface detail as possible, avoiding any background depth of field, as this has been shown to provide good reconstruction results (Zhang et al., 2016; Jiang and Jiang, 2017). Individual LW pieces are identifiable, and OFM is resolved at <10 mm (Fig. 1). Fig. 5a and b show the orthomosaic

Table 1

Camera specifications used for data collection in the field.

	GoPro	Huawei Nova 2i
Model	Hero3 Black Edition	RNE-L22
MP	12	16 + 2 (secondary rear camera)
Format	JPEG image	JPEG image
Sensor type	CMOS	CMOS BSI
Sensor Dimension (mm)	6.17 × 4.55	4.939 × 2.469
Focal length (mm)	2.98	4.00
35 mm focal Length (mm)	15	27
ISO range	100 to 154	50 to 100
Exposure range (sec)	1/120 to 1/447	1/50 to 1/128
F-stop	2.8	2.2

with overlapping images and the oblique orientation of the camera during acquisition, moving in a spiral trajectory around the LW accumulation covering 360°.

3.3. Point cloud processing

Photogrammetric processing was carried out using a commercially available SfM software package, Pix4DMapper (Pix4D Switzerland, 2018). Pix4D was selected for its user-friendly interface and workflow. Pix4D provides a coherent metadata and data set, including all images, camera models, point clouds, meshes, measurements (e.g. volume estimation) and a comprehensive technical quality report.

After initial processing (Step 1, Fig. 6 and Table 2), including point matching and point cloud generation, internal and external camera parameters were iteratively adjusted. This is done by loading automatically evaluated and optimised camera details into the Image Properties Editor and setting the principal points for x and y of the centre of the image. Using the BA technique, the software can determine the intrinsic camera parameters, such as lens characteristics, and the extrinsic camera parameters, such as positional information (Eltner et al., 2016). Our procedure continues with reprocessing of the first step, before the generated tie points are scaled in Pix4D according to the previously placed scaling bars. An arbitrary coordinate system was used, with the x-axis aligned to the flow direction.

The reoptimisation process incorporates prototype dimensions from scaling and orientation input into the point cloud model. The point cloud densification (Step 2) was then carried out, and a Digital Surface Model (DSM) was generated (Step 3), which is required to develop a volumetric model. The densified point cloud model provides the basis for meshing and surface reconstruction techniques described below. All software settings for our Pix4D workflow are listed in Table 2. We used a desktop PC with Windows 7 64-bit, 16GB RAM, i7-6700 3.40GHz CPU and a NVIDIA Quadro K600 graphic card, resulting in processing times of ≈ 20 h for a dataset with 72 12-MP photos.

Following the densified point cloud generation, the LW accumulation was isolated from the rest of the point cloud model using manual segmentation tools in CloudCompare, and cleaned from outlier points for further processing steps, including surface reconstruction. The final bounding dimensions for the LW accumulations in the point cloud model were 4.5 × 5.8 × 2.4 m (Whakatiwai River) and 3.3 × 3.8 × 1.8 m (Hapuku River).

3.4. Point cloud meshing

The point clouds normal were computed using Meshlab's 'Compute normal for point set' function, employing 10 neighbour points and a view direction toward the upward vertical to achieve best results. For surface reconstruction, we employed both (1) explicit triangulation methods and (2) implicit modelling of the point cloud in order to resolve the woody material. Both methods have inherent advantages,

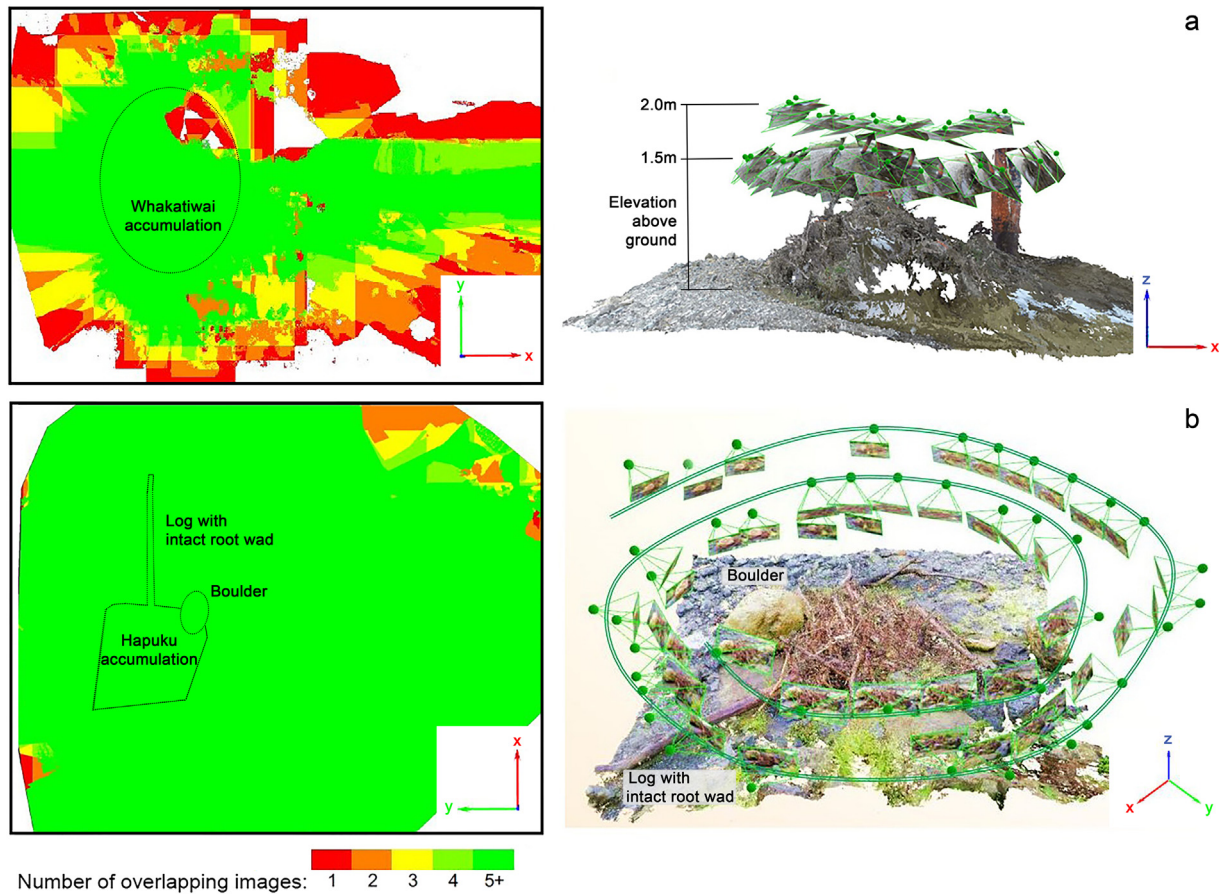


Fig. 5. Image overlap and the corresponding organic material accumulation for the Whakatiwai River (a) and the Hapuku River (b). Green indicates areas with five and more overlapping images, facilitating the generation of high-quality point cloud models. Orange indicates the minimum number of two overlapping images required for SfM photogrammetry. The black dotted lines represent the organic material accumulation, showing an area of low overlapping images for the Whakatiwai accumulation, which was partly inaccessible due to water (a), and full overlap for the Hapuku accumulation (b). Both organic material accumulation models (on the right) show oblique camera positions, obtained spirally around the object at an elevation of 1.5 to 2.0 m.

and have been employed in various geoscience applications (Frank et al., 2007; Yang et al., 2019).

The Delaunay triangulation and Voronoi diagram algorithm (Mitra and Nguyen, 2003) are used to compute points for unsampled locations, exactly in-between three points of the 3D point cloud. These methods are considered to be 'explicit', as they employ the input points to represent the surface. According to the newly computed points, one surface plane is created when connecting the computed points with each other. The Voronoi diagram builds up on a grid of connections between the centres of the circumcircles of the previously computed points from the Delaunay triangulation (Amenta and Bern, 1999), as featured in Pix4D.

The screened PSR (Kazhdan et al., 2006; Kazhdan and Hoppe, 2013), featured in MeshLab, uses the Poisson equation for computing the best-fit surface for a dense point cloud model, using a sparse set of points instead of the full area. This method belongs to the 'implicit' family of techniques that employ a function that is fit to the point cloud. Implicit techniques suffer from difficulties in capturing discontinuities, such as edges and corners, which may lead to artefacts in the resultant model. Despite this, the PSR method offers the best chances of minimum holes and mesh distortions over a complex point cloud. Altogether we used three meshing approaches:

- (i) A simplified mesh model based on Delaunay triangulation was generated using Pix4D. This mesh was generated on a restricted number of 10^6 faces in total (considering the entire point cloud model). Resolution was kept as default with an octree depth of 12 over a texture size of 8192×8192 pixels. The isolated LW

accumulations consequently show about half a million faces ($7 \cdot 10^5$ faces for the Whakatiwai River and $4 \cdot 10^5$ faces for the Hapuku River).

- (ii) The Delaunay triangulation (nearest-neighbour triangulation) with Voronoi filtering in CloudCompare (CloudCompareV2, 2016) is used for a xy-plane with triangulation on the point clouds' convex hull. The maximum length for triangle edges is set to 0.1 and it produces a 3D mesh structure based on the projected 2D point cloud (xy-plane) in this Delaunay 2.5D approach.
- (iii) For PSR (Kazhdan and Hoppe, 2013) in MeshLab (Cignoni et al., 2008), a reconstruction depth of 12, with an adaptive octree depth of 5, has been selected to achieve the best meshing results. The scaling factor is set to 1.0, with a minimum number of 5 samples.

All our meshes were filtered for isolated pieces, duplicated or unreferenced vertices, and zero area faces in MeshLab, allowing a proper volumetric computation of the generated 3D LW accumulation models.

3.5. Volumetric techniques

Volumes of our 3D point cloud and mesh models were computed via two software workflows: a predefined Pix4D tool 'Volumes', and CloudCompare's 'Compute 2.5D Volume' tool. The volume domain

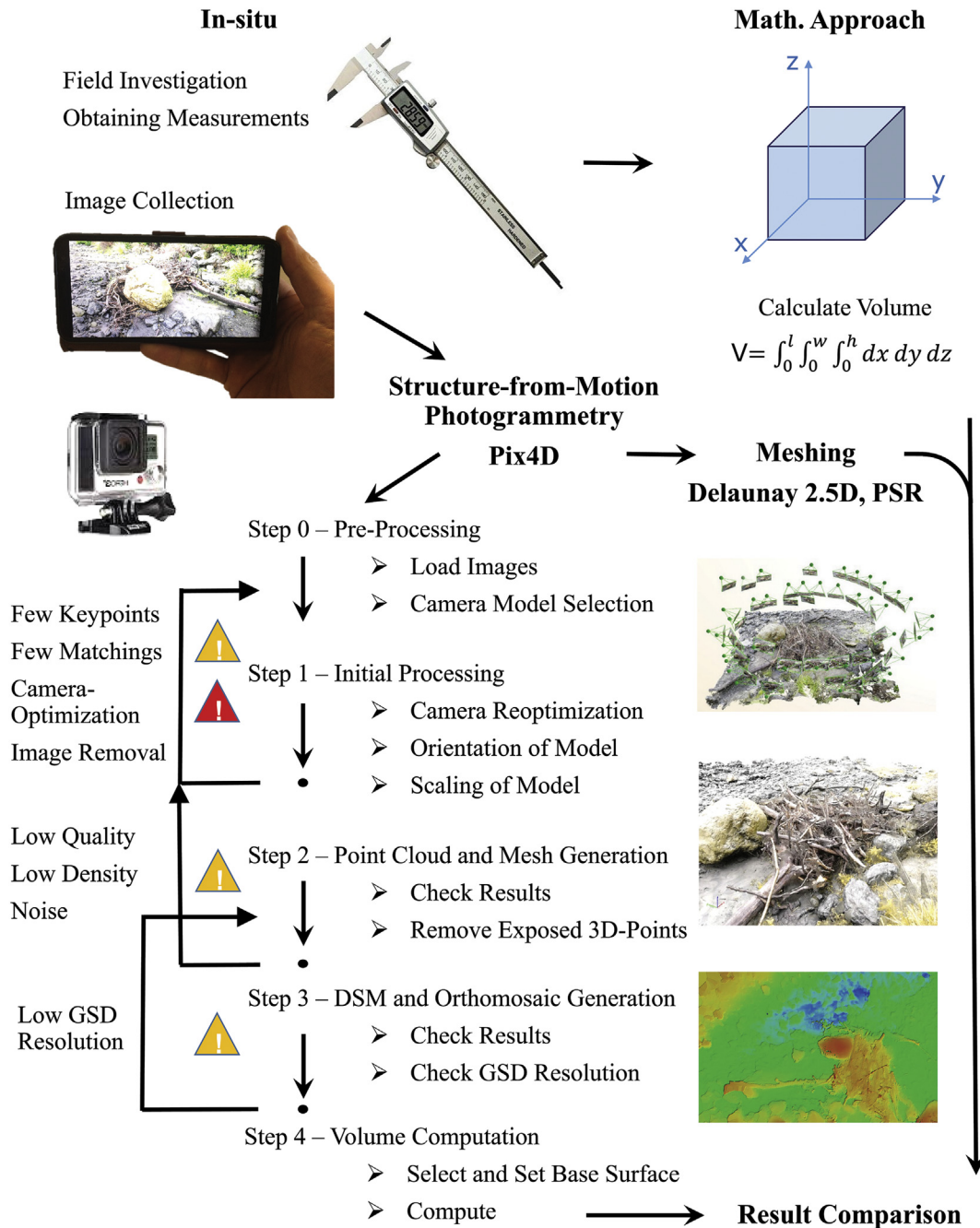


Fig. 6. SfM photogrammetry workflow.

consists of the octree subdivided to its finest level (10) in CloudCompare and with the standard resolution setting (12) in Pix4D. The volume is discretised into voxels, and estimated according Eq. (1). Model resolution is equivalent to the ground sampling distance (GSD), the product of the length (L_i) and width (W_i) of a basal surface cell. The vertical dimension (H_i) is the distance from the lower bounding basal surface to the top of the mesh model.

$$V_{p4d} = \sum_i L_i \cdot W_i \cdot H_i = \sum_i GSD_i^2 \cdot H_i \quad (1)$$

An essential modelling question involves specification of this lower basal surface, as well as any lateral boundaries (e.g. pier column, boulders). There are potentially significant uncertainties of this lower boundary between the wood accumulation and bed substrate. Depending on the inferred characteristics of the subjacent surface (e.g.

floodplain, bank, bedform), one can either specify a plane or an undulating bed that best matches the observed topography. This lower surface may be further obscured by deep/muddy water, overhanging wooden pieces and reflections, making interpolation difficult. Lateral boundaries may be further refined by trimming the model using geometric primitives, such as wedges, ellipsoids, cylinders and cones.

Volume estimates in CloudCompare are generated using the 2.5D volume computation tool. This tool allows the user to compute volumetric information of the generated meshes in Pix4D, CloudCompare and Meshlab by subtracting a reference surface (based on a custom defined footprint area). Similar to the algorithm applied in Pix4D, the volumetric tool in CloudCompare also uses an elementary parallelepiped with corresponding footprint area that is multiplied by the difference in height (CloudCompare, 2018). The grid step is set to a minimum of 0.001 m, and empty cells between the top of the mesh and the basal

Table 2

Data acquisition and Pix4D software processing settings and times.

Process	Clarification	Setting	Processing time
Data Acquisition In-Situ	Obtain images and dimensions of the LW accumulation		1–2 h
1.Initial Processing	Key Image Scale	Full	6–8 h
2.Point Cloud and Mesh	Point Cloud Densification -Point Density Image Scale	High (Slow) Multiscale, 1 (Original image size, Slow) Medium Resolution (8192 × 8192)	9–13 h
3.DSM and Orthomosaic	Default except of Counter Lines	DXF (El. Interval: 0.10)	1–2 h

reference surface are interpolated. Empty cells are kept at minimum height for the 3D LW accumulation model. This tool samples the same number of points on the mesh as on the original point cloud. The basal surface for the Whakatiwai accumulation includes a planar bottom and a cylinder for the adjacent bridge pier. The Hapuku model has a wavy surface that is consistent with the local surveyed topography; points representing the large boulder were cropped out.

As a check on the level of precision gained in our volume models, we developed a geometrical model of the LW accumulation for each field site using primitives in CAD to approximate the woody elements within the organic material formation. Volume estimates from the geometrical models are compared to the three mesh models. At the Whakatiwai River, the deposit most closely resembles a cone, built up at the bridge pier, effectively a cylinder. The dimensions of the organic material accumulation were obtained from measurements in the field (Fig. A.1). The cylindrical volume of the bridge pier, $r = 0.20$ m and $h = 1.10$ m, is subtracted from the cone model, $r = 1.90$ m and $h = 1.10$ m. All measurements from the Whakatiwai field site are based on the predominant water level elevation. The resulting prototype volume ($V_{W,pro}$) was estimated using Eq. (2), showing an approximation to prototype geometries.

$$V_{W,pro} = \frac{\pi \cdot r_{cone}^2 \cdot h}{3} - \pi \cdot r_{pier}^2 \cdot h \quad (2)$$

A trapezoidal prism was chosen to represent the organic material accumulation at the Hapuku River. The Hapuku accumulation (Figs. 3 and A.2) shows similar dimensions to the Whakatiwai. Both accumulations

are relatively small, consolidated and consists of large quantities of OFM (Fig. 4). A prototype volume approximation of the Hapuku accumulation ($V_{H,pro}$; Eq. (3)) is obtained by using an irregular trapezoid; $a = 0.85$ m, $b = 2.00$ m, $l = 3.00$ m and $h = 0.40$ m, determined from measurements in the field.

$$V_{H,pro} = \frac{a + b}{2} \cdot l \cdot h \quad (3)$$

None of the volumetric models account for the porosity of the deposit. Essentially the photogrammetric model provides better capture of the complex surface, but the internal structure of the deposit remains obscured.

4. Results

4.1. Point cloud results

The Whakatiwai organic material accumulation model had an average of 45,640 keypoints/image, whereas 37.4% of these keypoints in every image are matched points (Table A.1) for a median of 17.06 matched 2D keypoints/image. The dense point cloud model of the Whakatiwai accumulation, Fig. 7a, had almost $37 \cdot 10^6$ 3D points. GSD for the organic material accumulation model at the Whakatiwai River was 1.9 mm. The volume domain of the point cloud model at the Whakatiwai River encompasses roughly $4.5 \times 5.8 \times 2.4$ m, or 63 m^3 . This results in a point density of $1.25 \cdot 10^6$ points/ m^2 projected area, or $5.15 \cdot 10^5$ points/ m^3 (Table A.2).

By contrast, the Hapuku organic material accumulation dense model had $44.5 \cdot 10^6$ 3D points (Fig. 7b). The volume domain here was roughly $3.3 \times 3.8 \text{ m} \times 1.8$ m, or 23 m^3 . Thus, the accumulation model at the Hapuku River shows an average point density of $3.56 \cdot 10^6$ points/ m^2 over the projected platform area or $1.96 \cdot 10^6$ points/ m^3 (Table A.3).

The resolution achieved in the model ($1.96 \cdot 10^6$ points/ m^3) readily resolves distinct particles larger than 1.3 mm. Despite the high level of detail in both organic material accumulation models, occasional protruding branches are not reconstructed properly.

Pix4D provides a statistical assessment of camera correction required within the model, in order to counteract the effects of lens distortion. The initial, un-optimised imagery from the GoPro camera had a camera error of 0.01%. This high-quality correction is enabled by lens correction factors stored in the Pix4D lens database. The Huawei model is not in this database, with a difference between initial and optimised error of 3.64%, revealing the influence of lens correction factors on model quality. In the Quality Report, Pix4D suggests re-optimisation for project with errors exceeding 5%. Nevertheless, we



Fig. 7. Point cloud models of the organic material accumulation at the Whakatiwai River (a) and at the Hapuku River (b).

loaded the optimised camera parameter into the image property editor and reprocessed the project. The reoptimisation process resulted in identical parameters for initial and optimised focal length, a 100% optimisation of our smartphone camera.

4.2. Meshing results

For both point cloud models, three different mesh types were generated (see Section 3.4 above) for comparison of volumetric measurements within each organic material accumulation. The Whakatiwai organic material accumulation had an average of $2.84 \cdot 10^6$ faces/m³ (Table A.2) and the Hapuku site had an average of $6.97 \cdot 10^6$ faces/m³ (Table A.3). The implicit Poisson surfaces tended to have the highest density of faces, while the explicit Delaunay meshes had roughly 20–30% fewer. The Pix4D output had by far the lowest density, typically by about two orders of magnitude (Table A.3). We selected a maximum resolution for the Pix4D volume model of $1 \cdot 10^6$ faces/m³.

Fig. 8 shows a rendering of the organic material accumulation Point Cloud (a), Simplified Pix4D mesh (b), Delaunay 2.5D mesh (c), and PSR mesh (d) at the Hapuku River. The original point cloud is displayed in Fig. 8a, showing a very high level of detail. In particular, small wooden pieces and OFM are resolved at a high point density. The screened PSR has shown best results, resolving sticks and twigs down to 1.3 mm in the model. As can be seen in Fig. 8d, non-optimised point normal computation results in bubble formation at the end of the protruding branches. Furthermore, thin strands of wood and other individual particles emerging from the model are inaccurately captured in the transition zone between the channel bed and the organic material accumulation, whereas the other mesh models do not show any such artefacts resulting from point normal estimation. The simplified Pix4D mesh (Fig. 8b) has shown a high level of detail, considering the mesh was built from only a fraction of the faces of PSR and Delaunay 2.5D mesh. In the simplified Pix4D mesh model, wooden particles with a minimum diameter of 3.5 mm could be fully reconstructed. The model

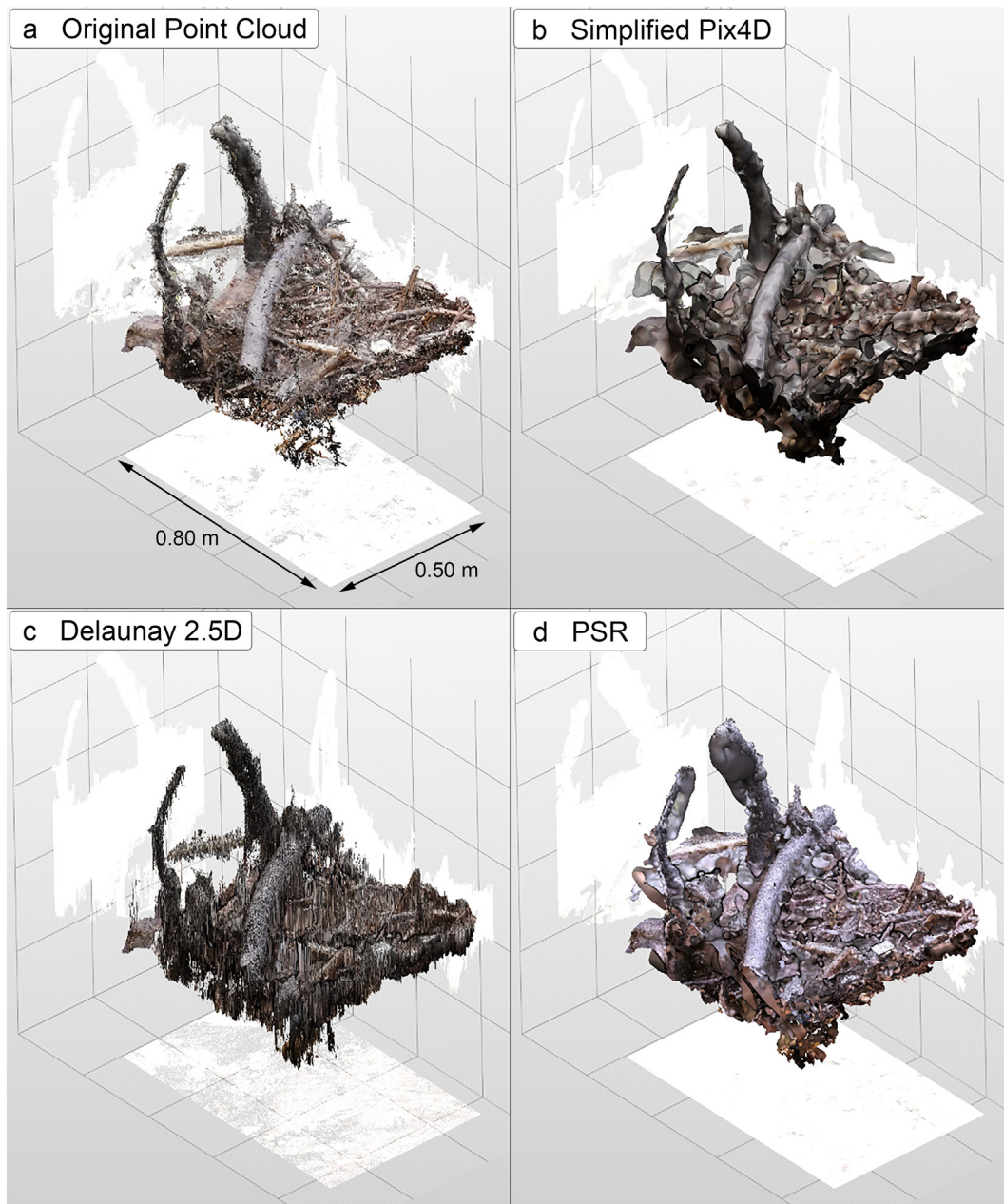


Fig. 8. Organic material accumulation from the Hapuku field site. The selection shows a 0.80×0.50 m section, displaying the original point cloud (a), the simplified Pix4D mesh (b), the Delaunay 2.5D mesh (c) and the screened Poisson Surface Reconstruction (PSR) mesh (d).

further shows a relatively smooth transitioning between individual emerging particles and organic material accumulation, indicating ideal point normal orientations. A limited number of wooden particles can be identified in the Delaunay 2.5D mesh (Fig. 8c), where it is assumed that computed edge length strongly influences model resolution.

4.3. Volumetric results

An estimate of the total wood volume within each of the two accumulations was made by integrating the volume between the mesh and the basal bounding surfaces for each model type, as well as integrating the volume of the geometric primitive model. Fig. 9 shows orthoimages of the organic material accumulations in Pix4D. The base surface was set to an elevation in accordance with the coarse gravel bar upstream and the fine material in the downstream reach of the accumulation.

Results from the Pix4D volumetric tool were set as the reference volumes for each site in order to evaluate the performance of the photogrammetry software package, Pix4D, for volume estimates. With a computed GSD resolution, $L_i \cdot W_i$, of 3.61 mm^2 the Pix4D Volume (V_{Pix4D}) for the Whakatiwai organic material accumulation was 3.75 m^3

(Table 3). The mathematical approximation using geometric primitives resulted in a volume of 4.02 m^3 .

At the Hapuku River site, a GSD of 1.3 mm was achieved, for a base raster resolution of 1.69 mm^2 . A total volume (V_{Pix4D}) of 1.54 m^3 was obtained. An average accumulation height of 0.40 m was estimated in the field, and this was used to generate a mathematical trapezoidal model for the Hapuku organic material accumulation that was used for volume approximation. The resultant volume was 1.71 m^3 .

CloudCompare was used for the calculation of point cloud and mesh volumes. The original point cloud models achieved best approximation of the reference volume computed with the Pix4D volume tool. The point cloud volume for the Whakatiwai accumulation is 3.65 m^3 and 1.50 m^3 for the Hapuku accumulation, both showing a variance of 2.6% from the reference volume. The Poisson model would appear to have generated the most accurate surface reconstruction; however computed volumes vary from 3.6% (3.89 m^3) at the Whakatiwai River up to 18.8% (1.83 m^3) at the Hapuku River. Delaunay 2.5D mesh shows largest volume deviations, with $>40\%$ difference, for both organic material accumulation models. Due to these large differences, volumes generated based on Delaunay 2.5D mesh were considered to be invalid for standard deviation and error estimates. Details of all organic material accumulation volume computations for the Whakatiwai and the

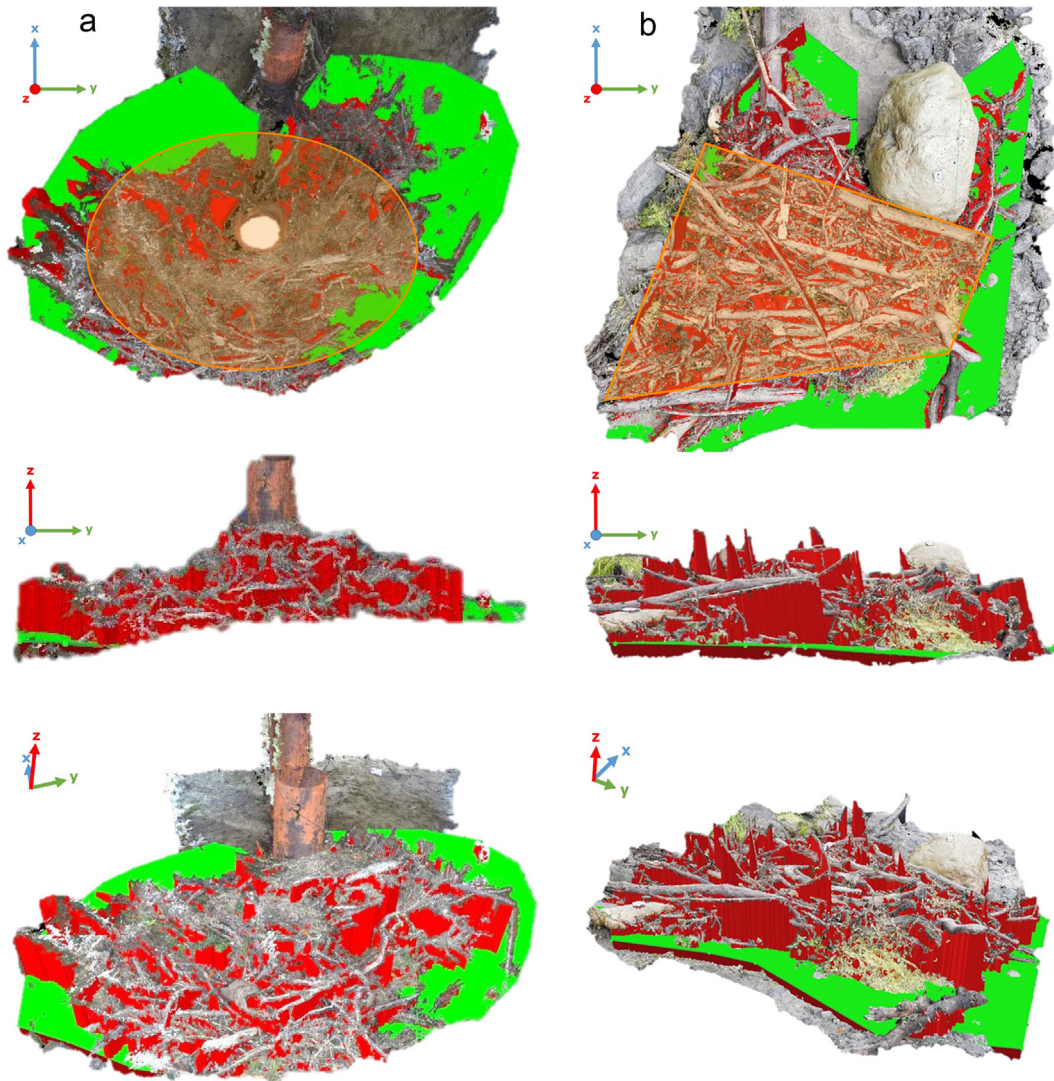


Fig. 9. Volume computation of the organic material accumulations using the Pix4D volume tool. On the left (a): Whakatiwai and right (b): Hapuku River; Green: shows the basal surface for volume computation, red: the vectors for volume estimation, and orange: the mathematical cone model left and trapezoidal prism model right. Top view, front view and side view perspective from the top to the bottom.

Table 3

Overview of the results from measured and computed accumulation volumes. The volume measured with the Pix4D Volume Tool represents our reference value for volume comparison. Furthermore, measured dimensions from the field are presented together with computed volumes, using a Mathematical Approximation, the Original Point Cloud and three meshes of the organic material accumulation at the Whakatiwai and Hapuku River.

Volume computation variant	Whakatiwai River	Hapuku River
Pix4D Volume Tool (ref. volume)		
Pix4D Volume Tool, V_{P4D} (m ³)	3.75	1.54
Mathematical Model	Cone	Irregular trapezoid
Length (m)	$r_{acc} = 1.90$ $r_{pier} = 0.20$	$a = 0.85$ $b = 2.00$
Width (m)	–	3.00
Height (m)	1.10	0.40
Math. Approximation Volume, $V_{M.A.}$ (m ³)	4.02	1.71
Variance from V_{P4D} (m ³)	0.27 (7.2%)	0.17 (11.0%)
Point Cloud		
Original Point Cloud Volume, $V_{P.C.}$ (m ³)	3.65	1.50
Variance from V_{P4D} (m ³)	0.10 (2.6%)	0.04 (2.6%)
Mesh		
Simplified Pix4D Mesh Volume, V_{Spl} (m ³)	3.62	1.64
Variance from V_{P4D} (m ³)	0.13 (3.4%)	0.10 (6.5%)
PSR Mesh Volume, V_{PSR} (m ³)	3.89	1.83
Variance from V_{P4D} (m ³)	0.14 (3.6%)	0.29 (18.8%)
Delaunay 2.5D Mesh Volume, V_{Del} (m ³)	2.22	0.90
Variance from V_{P4D} (m ³)	1.53 (40.9%)	0.64 (41.6%)
Statistics		
Standard Deviation all	0.6580	0.3261
Standard Error all	0.2686	0.1331
Standard Deviation excl. V_{Del}	0.1662	0.1328
Standard Error excl. V_{Del}	0.0743	0.0594

Hapuku River are given in Table 3. The standard deviation and standard error of the mean are assessed relative to the volume measured with the Pix4D volume tool. The boulder captured in the Hapuku dataset was not considered for volume computation and removed from all point cloud and mesh models.

5. Discussion

5.1. Complex LW accumulations

The Whakatiwai accumulation was scanned using two GoPro Hero3 cameras equipped with fisheye lens. Due to the large field of view of the GoPro's fisheye lens ($\approx 115^\circ$), more background information was captured than when using a smartphone camera. This resulted in a bounding box computed for the Whakatiwai point cloud model ($243 \times 67 \times 13$ m or $211,653$ m³) that was six times larger than the Hapuku point cloud model ($137 \times 38 \times 9$ m or $46,854$ m³), even though the wood accumulations were of similar size. In contrast to more typical nadir images (obtained from airborne cameras), oblique images have non-orthogonal overlap characteristics, since the movement is not longitudinal but rather radial around the object (Micheletti et al., 2015a). When obtaining images with shallower angles relative to the horizontal, variation in depth increases for images taken further away from the object (Smith and Vericat, 2015; Pix4Dmapper, 2018). This results in fewer available key points and a low percentage of image information contributing to the matching processes; this effect came into play in the present study. The Hapuku accumulation shows almost twice the number of computed 3D densified points as the Whakatiwai accumulation model (Table A.1). In general, a high density point cloud and good overlapping matches (Fig. 5) are indicative of minimal influence from the background field.

Both of our reconstructed organic material accumulation point cloud models show similar resolution and an extremely high point density, reflecting a key strength of Pix4Dmapper, with close point spacing (Alidoost and Arefi, 2017) and high spatial accuracies (low noise) (Burns and Delparte, 2017). These high-quality point cloud models

ensure that individual particles at the accumulation surface are resolved with a resolution in the range of 10^{-4} to 10^{-3} m. To resolve a gapless surface structure in the model, a high level of detail is required, especially when large amounts of OFM are present (Fig. 4). Some of the protruding branches around the main organic material accumulation are not properly reconstructed, as they got lost at the stage of tie point processing and filtering. Reconstructed elements (minimum diameter of 10 mm), however, show a high level of detail, adding significant information about LW accumulation composition, shape, geometry as well as surface texture and roughness.

Based on the meshing results, the simplified Pix4D mesh presents a good compromise between quick processing times and a high level of detail. This is the intrinsic challenge in photogrammetric surveying: finding a suitable compromise between better quality imagery acquisition, faster processing routines and very high resolution data output (Micheletti et al., 2015a). The resultant models have a lower number of faces, but present a reasonably accurate surface reconstruction. The simplified Pix4D mesh also has the benefit of accurate point normals, avoiding bubble formation (Boltcheva and Levy, 2016) at protruding branches, a problem observed with screened PSR (Fig. 8d).

For both of our organic material accumulation models, the PSR method, completed in MeshLab, generated the highest number of faces; almost twice the number of faces as original points in the model. The number of computed faces and the quality of the generated surface depends strongly on the defined octree depth (Maiti and Chakravarty, 2016), which was set to 12 for surface reconstruction of the organic material accumulations. Our Delaunay 2.5D triangulation resulted in about 1.5 times more faces than points, however, it showed less detail in surface reconstruction, formed by poorly-shaped triangles showing sharp edges (Gao et al., 2013), and large deviations in volume of the accumulation models.

5.2. Volumetric computations

In total, six individual volume estimates were developed for each of the Whakatiwai and the Hapuku organic material accumulations. Volume comparisons within each of the accumulation models are based on the reference volume (Pix4D Volume Tool) that is computed with the volumetric tool in Pix4Dmapper. This reference volume is then compared to the corresponding point cloud model, three mesh models and the mathematical approximation. The Delaunay 2.5D mesh, which has been computed with a maximum edge length of 0.1, showed the largest deviation. For both organic material accumulations, the application of the Delaunay 2.5D mesh resulted in volumes that were 40% less than the corresponding reference volume. These large deviations observed in our results may be explained by a lack of truly 3D geometrical structures (limited to 2.5D), as standard Delaunay methods do not consider the Z-value of points properly (Verbree and Van Oosterom, 2003), and are further restricted because of a pre-defined maximum edge length for mesh generation (CloudCompare 2.5D, 2016).

Results from both original point cloud models tended to show a slight underestimation of volume (2.6%), relative to the reference volume. The simplified Pix4D mesh showed a deviation of <7%. As shown in Table 3, the PSR mesh tended to have a higher volume (up to 19%) than others, even though (qualitatively) it seemed to follow the contours of the point clouds more closely than others (Fig. 8). Both of our mathematical approximations overestimated the computed volume by up to 11%. The original point cloud and Pix4D volume tool estimates are consistent with these results, which are all in a range of <7% deviation from the reference, except the PSR mesh for the Hapuku accumulation, revealing an overestimation by 19%. The overestimation of the PSR mesh on the Hapuku river is possibly related to the larger number of protruding branches, which are prone to forming a hull (bubbles) during the meshing process (Matsuda and Ukita, 2011; Boltcheva and Levy, 2016), leading to an inflated volume estimate. The results provide some confidence in the use of the reduced and simplified output from

the Pix4D volume tool. Our findings provide some insight into complex geometries of LW accumulations (thin isolated strands of wood, sharp corners) that can cause the meshing algorithms to fail.

There are two further important sources of error: (1) the alignment of the lower boundary surface is critical, and thus it is important to reproduce this surface as faithfully as possible; and (2) the software follows strict algorithms in regards volume computation, which can lead to failure when applied to particularly complex LW accumulations. A general problem here is the assessment of volume within material that sticks out from the woody mass. Empty space between ground and protruding branches is not dealt with adequately in a '2.5D' approach. The software locates the farthest point, perpendicular to the base surface and computes the volume for each GSD unit (Pix4Dmapper, 2018), without taking into account any further surface information of the accumulation body. This error strongly depends on the volume of long, thin protruding geometry (branches), but also on point cloud quality with non-filtered outlier points above the base surface. The error emerging from outlier points is limited due to the fine resolution of the point cloud and the fact that only a small number of points can be recognised exactly perpendicular to the base surface plane and GSD unit.

The average interpolation error of the Pix4D volume tool has been assessed to be 1.5 times the GSD in the z-direction (Pix4Donline, 2018), with a maximum error of 2.5 mm times the footprint area of the accumulation. Thus, this particular error is negligible, due to the high resolution of the point cloud model and the error introduced via base surface alignment. Expressed as a volume, the upper bound error of 2.5 mm difference in elevation would result in a

deviation of $\pm 0.01 \text{ m}^3$. Considering this magnitude of error, the SfM photogrammetry methodology presented here for volume computation represents an improvement from the previously applied volume estimate techniques, such as counting and measuring individual logs (Cordova et al., 2006; Brown et al., 2014; Dixon and Sear, 2014), or applying a rectangular model for air-wood volume estimation (Boivin et al., 2015).

There are time and cost benefits to be gained from the rectangular (parallelepiped) approach to estimate volumes directly in the field (Boivin et al., 2015), which can be obtained within a few minutes after measuring the three axes. In contrast, it takes about 21 h to acquire data and execute SfM volume computations (Table 2), although with significant gains in volume accuracy. Pix4DMapper is currently slightly more expensive than Agisoft Photoscan (Agisoft LLC Russia, 2018), however, freely available SfM photogrammetry solutions such as VisualSfM (Wu, 2013; VisualSfM, 2018) and SfM-Toolkit (Astre, 2015) can be used for this stage in the processing pipeline to keep expenses to a minimum. Processing times can be reduced drastically by subsampling point clouds after dense cloud generation, with the advantage of preserving key surface characteristics (Wu and Kobbelt, 2004; Tazir et al., 2016). One may also subdivide complex point clouds into multiple segments for processing (Miknis et al., 2016); further studies are needed to evaluate how volumetric error varies as a function of model detail. Wróżyński et al. (2017) computed volumes of stockpiles using SfM photogrammetry and achieved processing times of less than one hour, inclusive of data acquisition. These processing times may also apply for SfM photogrammetry-based LW volume estimations, although wood accumulations show more complex surface texture.

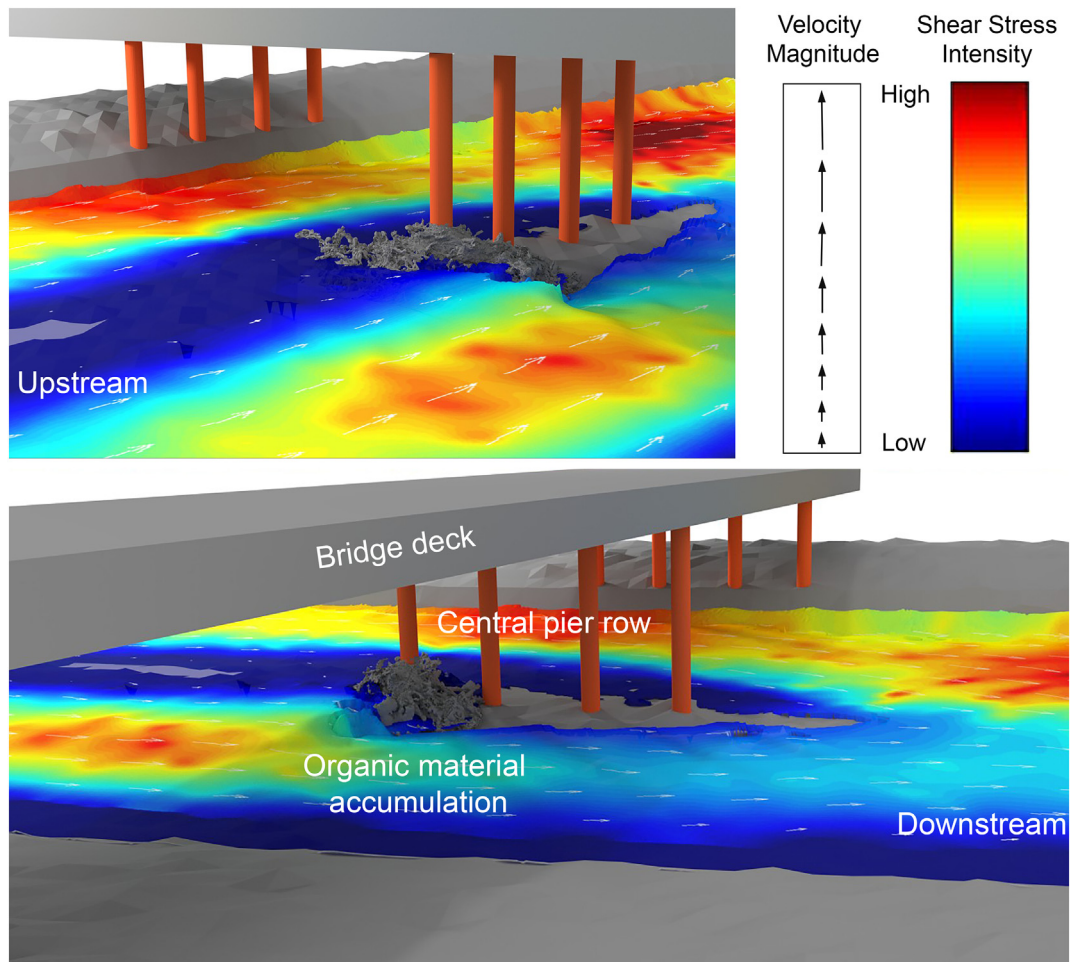


Fig. 10. Simulation of the effects on channel morphology using the Whakatiwai accumulation model embedded into a Delft3D (2011) environment.

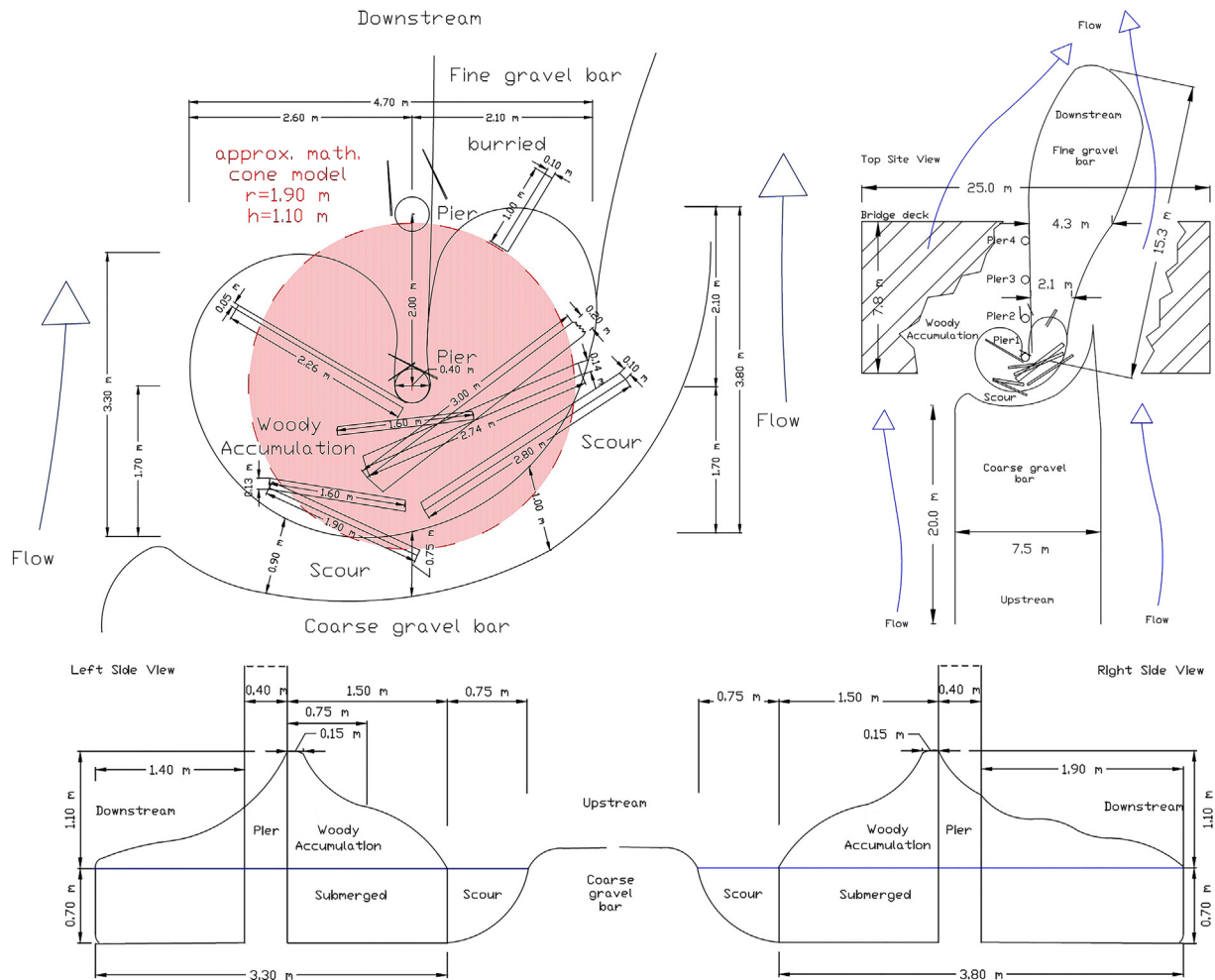


Fig. A.1. Top view of the Whakatiwai organic material accumulation, top left side. The transparent red circle represents a cone with a height of 1.10 m and a base diameter of 3.80 m in approximation to the prototype LW accumulation. Site view of the Whakatiwai River with bridge and gravel bars, top right side, and two illustrations from the left and right perspective of the LW accumulation.

5.3. LW accumulation assessment

There is a need for accurate, detailed, and objective techniques for estimating wood volumes in a variety of management contexts. Conventional large-scale surveying methods have gained popularity for wood budgeting applications (Ulloa et al., 2016; Tonon et al., 2017), yet with increasing distance between sensor and wood the spatial model accuracy decreases (Fig. 1). Challenges arise when LW pieces are smaller than the achieved model resolution (Marcus et al., 2003; Tonon et al., 2018). Therefore, a combination of field- and aerial surveying could improve volume estimates significantly (Boivin et al., 2017).

Phillips et al. (2018) outlined the need for a better quantitative capture of the effects from post-harvest debris flows, in order to better inform predictive models. The same is required for assessing wood inputs from natural forest disturbance such as fire, landslides and avalanches, or heavy storm events. This is the current focus of numerous LW studies (Thevenet et al., 1998; MacVicar et al., 2009; Ruiz-Villanueva et al., 2014b; Steeb et al., 2017; Sanhueza et al., 2018), however, the mass and volume of wood still remains rarely described (Ruiz-Villanueva et al., 2019). Although a broad variety of volumetric surveying methods for LW sources exists; including LiDAR (Kasprak et al., 2012; Atha and Dietrich, 2016), aerial photogrammetry (Boivin et al., 2017; Sanhueza et al., 2018) and manually conducted measurements (Piegay, 1993; Boivin et al., 2015), precise quantification of LW sources remains challenging. Mazzorana and Fuchs (2010) found that transported wood act as a potential risk amplifier during flood events,

for which reason a fundamental knowledge of the available wooden quantities in vulnerable fluvial systems is essential.

Risk analyses are a widely discussed topic in the LW community, with various analysis proposed to better understand the probabilities and process linkages that bring wood from the hillslope to the river (Comiti et al., 2016). Risk factors can be better characterized by carrying out volumetric surveys of wood accumulations along this gradient (Zischg et al., 2018), before the occurrence of 'LW incidents' (Cave et al., 2017). Our methodology provides an example application for the assessment of LW volume at a high resolution, as suggested by Hübl et al. (2002), but also for governmental authorities that require forestry and earthworks plans, where SfM photogrammetry can be used to assess LW quantities, which are available at a field site and at risk for entering a stream system during forest harvesting operations in a watershed (Reddy, 2017). The technique can be widely and rapidly deployed, with data collection and processing done within 24 h and can be applied to emerging assessment frameworks, such as the Risk Assessment for the National Environmental Standards for Plantation Forestry (Ministry for Primary Industries, 2017).

Due to the fact that individual LW pieces and entire accumulation structures in a stream can alter channel morphology (Mosley, 1981; Wohl and Scott, 2017) and discharge behaviour (Gschmitter et al., 2017; Schalko et al., 2018), all affecting safety aspects in regards discharge conveyance and resilience of river-crossing infrastructure, investigations on LW accumulation volume (Lienkaemper and Swanson, 1987), geometry (Cordova et al., 2006; Dixon and Sear, 2014), and

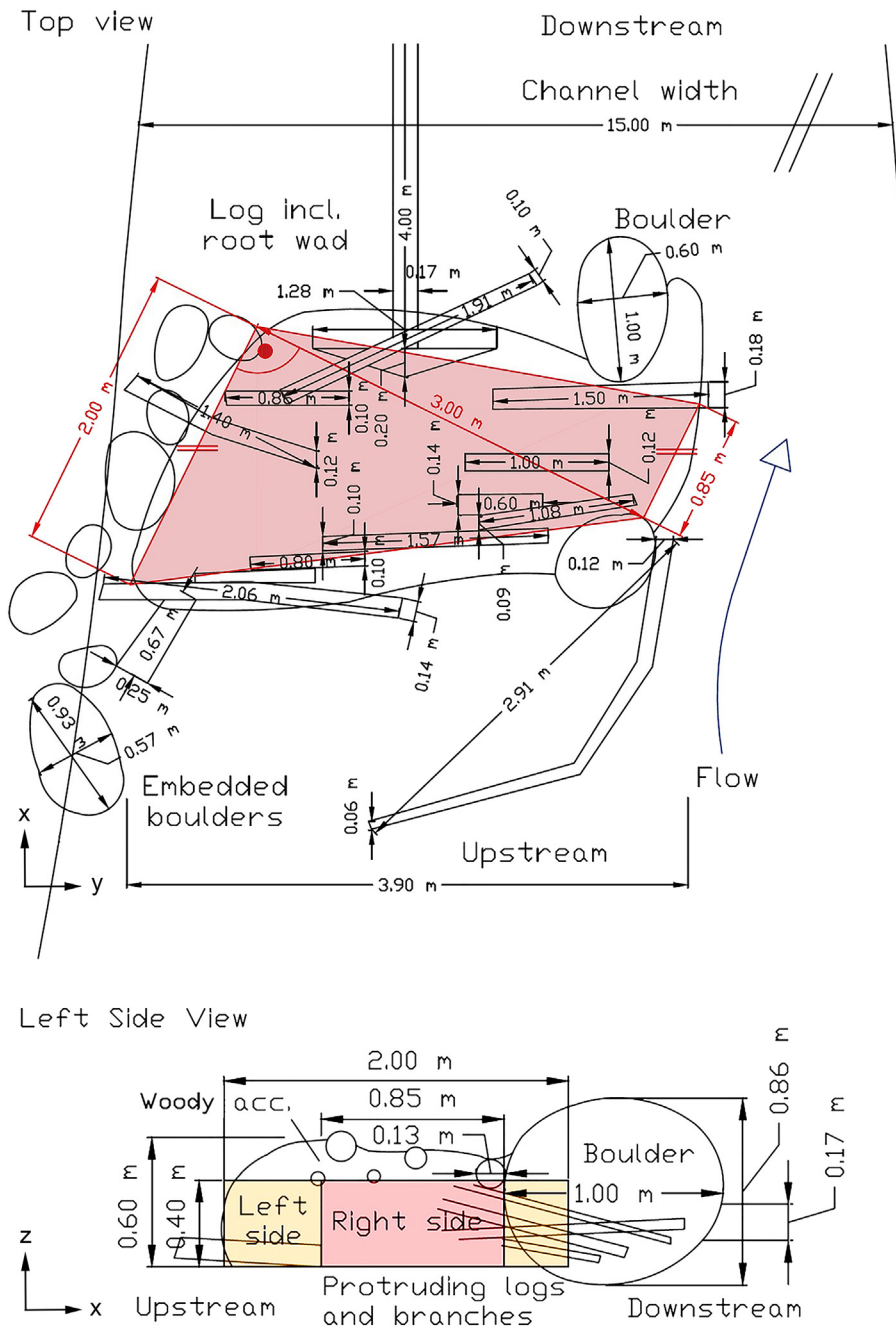


Fig. A.2. Top view of the Hapuku organic material accumulation, top. The transparent red trapezoid represents a mathematical approximation to the prototype LW accumulation. A side perspective of the LW accumulation is shown in the bottom sketch.

orientation in the channel (Abbe and Montgomery, 2003; Ruiz-Villanueva et al., 2016) are essential. Detailed surveys providing high-resolution data of LW accumulations, however, are infrequently reported. Thus a lack of meaningful assessment opportunities arise in the field of LW research. The introduced method provides a powerful and compact tool for accurate assessment of existing LW structures and wood sources in the riparian zone to gain information about (i) wood budgeting and the quantity of available wood (Benda et al., 2003; Schenk et al., 2014; Sanhueza et al., 2018; Tonon et al., 2018) on a basis of pre- and post-flood assessment, (ii) residence times LW accumulation volume and development during flood events, when organic material is removed or deposited (Sanhueza et al., 2018), and (iii) accumulation structure and orientation with respect to the flow (Daniels, 2006; Ruiz-Villanueva et al., 2016). This is needed to estimate effects on hydraulic flow behaviour and impacts on channel morphology.

Improving the compositional information, such as relative proportions of wood, branches, sediment, organics and pore space (Piegay, 1993; Boivin and Buffin-Bélanger, 2010; Schalko et al., 2018), is a major challenge in the quantification of LW accumulation assessment. The techniques presented herewith perform well in capturing the 'envelope' of the deposit, and providing a detailed record of the texture, yet estimates of deposit porosity remain biased toward the outer shell. Backwater effects, changes in channel morphology and drag forces on the accumulation body strongly depend on the ratio of void volume over total volume (Pagliara and Carnacina, 2010; Schalko et al., 2018; Schalko et al., 2019). Void volume may be determined from surface texture, which can be filtered for colours (Orru et al., 2016) (e.g. wood, grass, sediments) to broadly estimate compositional proportions. The mesh can be further manipulated, using techniques such as mesh skeletonization (AlRatrou et al.,

2018) in order to resolve major compositional members (tree stems, major branches) and collect statistical information on the geometrical arrangement of these structural items. Seitz et al. (2018) successfully demonstrated the application of a SfM photogrammetry workflow to estimate porosity of soil samples using a laboratory setup and water replacement methodology.

These previous studies on porosity estimates using SfM methodology can significantly contribute to incorporating LW accumulations in computational fluid dynamics (CFD) modelling. Accurate 3D mesh models, and information about roughness parameters (Gippel, 1995; Manners et al., 2007), angularity (Lisle, 1986; Lai and Bandrowski, 2014), hydraulic losses (Knauss, 1995; Shields, 2001; Schalko et al., 2018) are furthermore of considerable importance for CFD modelling (Xu and Liu, 2017). Major advances have been achieved in recent years with the application of 2D (Ruiz-Villanueva et al., 2014a; Ventres-Pake et al., 2019), but also 3D LW computational models (Smith et al., 2011; Allen and Smith, 2012; Lai, 2016) to evaluate hydraulic flow behaviour. For example, a prototype accumulation model can be used for investigating the effects on flow and channel morphology in presence of a LW accumulation (Fig. 10). Low grid resolution can cause high distortions, numerical diffusion and instabilities (Allen and Smith, 2012) in CFD models, and so it is important to provide a smooth, yet sufficiently detailed model surface in order to capture the relevant process(es) without introducing resistance from mesh imperfections. The work pipeline we have presented here provides a number of options for developing a suitably detailed mesh for hydraulic simulations involving LW accumulations.

6. Conclusions

We developed detailed models of prototype organic material accumulations that can be used for accurate volume measurements and 3D modelling. We outlined the research need and we show that SfM photogrammetry offers significant improvement over existing approaches, such as volume estimation from observation and rough estimation based on single log dimensions, or parallelepiped approaches. We discussed the need for generating a detailed yet 'watertight' surface (no holes in the enclosing mesh) from an unorganized point cloud for the modelling of complex organic forms.

Appendix A

Table A.1
Pix4D point cloud statistics.

Camera model	GoPro Hero3 Black Edition	Huawei Nova 2i RNE-L22
River	Whakatiwai	Hapuku
Obtained Images	72 (2 × 36)	120
Resolution (pixel)	4000 × 3000	4608 × 2304
Calibrated images (%)	100	100
Initial Camera Optimisation (%)	99.99	96.36
Final Camera Optimisation (%)	–	100
Mean Key-Point/Image	45,640	55,059
Matching (matches/calibrated image)	17,061	15,029
Georeferencing	No	No
2D Keypoints Bundle-Block-Adjustment	1,188,967	2,029,796
3D Point Bund-Block-Adjustment	434,674	781,169
Mean Reprojection Error (pixels)	0.411	0.192
Number of 3D Densified Points for the total field site	45.9 · 10 ⁶	93.6 · 10 ⁶
DSM Resolution (mm/pixel)	1.9	1.3

The importance of using appropriate distance to the object for image capturing, collecting a sufficient number of images and using a suitably high-resolution camera sensor is highlighted. Furthermore, we review the workflow from point cloud generation in Pix4D to mesh generation, comparing three different meshing techniques (Simplified Pix4D, Delaunay 2.5D, and PSR), and point out relative advantages. It is shown that 2.5D techniques are affected by overhanging geometry; the Poisson techniques generate large artefacts in the presence of thin, poorly defined branches that protrude from the main accumulation; the simplified Pix4D model manages to avoid these pitfalls to generate a low-poly mesh that preserves important surface details. It was further found that the Pix4D volume tool slightly overestimates the volume of the initial point cloud model, by 2.6%, for both field sites. Using the PSR mesh provided the best overall result relative to the reference volumes. While we conclude that the original point cloud can be used for rapid volume estimates, a watertight hull is required for modelling applications that take into consideration surface texture and roughness.

The final results reveal that the meshing algorithm from Pix4D is superior to the other techniques in that it has a low poly count and a robust topology that is highly suited to volume estimation and rapid processing. The other techniques generated more highly resolved models, however, they also tended to have a very high number of faces, and more spurious features, relative to the initial point cloud. The user needs to assess the requirements for their analysis, with respect to model resolutions, processing times, and accuracy beforehand in order to achieve the best project outcome.

We suggest that the technique should be used to improve the workflow (and subsequent analyses) in the field, as well as in the laboratory, for a suite of LW assessment tasks in the course of wood budgeting, habitat characterisation, assessing sediment retention while looking at LW influence on river morphology, and potentially, modelling hydraulic interactions by implementing most realistic prototype accumulation models.

Acknowledgements

The Kaikōura field trip was funded by the Ministry of Business, Innovation and Employment (MBIE), as part of the Endeavour Earthquake Induced Landscape Dynamics (EILD) program. The authors thank the Water-worked Environments Research-Group for their support during the Hunua field trip.

Table A.2

Whakatiwai River organic material accumulation point cloud and mesh characteristics with densities for projected footprint area and accumulation volume.

Specification	Point Cloud	Simplified Pix4D	Delaunay 2.5D	PSR
Box dimensions LW accumulation				
x (m)	4.4893	4.3823	4.4893	4.6884
y (m)	5.8370	6.3464	5.8370	5.8370
z (m)	2.4187	2.5352	2.4187	2.4251
Area projected (xy)(m ²)	26.204	27.812	26.204	27.366
Volume (m ³)	63.379	70.507	63.379	66.364
Number of points	32,665,931	–	–	–
Number of faces	–	707,462	50,829,207	77,628,354
Density projected (points·m ⁻²)	1,246,610	–	–	–
Density projected (faces·m ⁻²)	–	25,437	1,939,7640	2,836,354
Density (points·m ⁻³)	515,405	–	–	–
Density (faces·m ⁻³)	–	10,034	801,986	1,169,728

Table A.3

Hapuku River organic material accumulation point cloud and mesh characteristics (without boulder) with densities for projected footprint area and accumulation volume.

Specification	Point Cloud	Simplified Pix4D	Delaunay 2.5D	PSR
Box dimensions LW accumulation				
x (m)	3.3034	3.2571	3.3037	3.4860
y (m)	3.7814	3.7647	3.7814	3.7814
z (m)	1.8222	1.2386	1.2533	1.2334
Area projected (xy)(m ²)	12.492	12.262	12.493	13.182
Volume (m ³)	22.764	15.188	15.657	16.259
Number of points	44,522,655	–	–	–
Number of faces	–	400,068	73,116,103	91,886,732
Density projected (points·m ⁻²)	3,563,951	–	–	–
Density projected (faces·m ⁻²)	–	32,626	5,852,799	6,970,707
Density (points·m ⁻³)	1,955,804	–	–	–
Density (faces·m ⁻³)	–	26,342	4,669,907	5,651,425

References

- Abbe, T.B., Montgomery, D.R., 1996. Large woody debris jams, channel hydraulics and habitat formation in large rivers. *Regul. Rivers Res. Manag.* 12, 201–221.
- Abbe, T.B., Montgomery, D.R., 2003. Patterns and processes of wood debris accumulation in the Queets river basin, Washington. *Geomorphology* 51, 81–107.
- AGISOFT LLC RUSSIA 2018. PhotoScan - photogrammetric processing of digital images and 3D spatial data generation.
- Alidoost, F., Arefi, H., 2017. Comparison of Uas-based photogrammetry software for 3d point cloud generation: a survey over a historical site. *ISPRS Annals of Photogrammetry, Remote Sensing and Spatial Information Sciences IV-4 (W4)*, 55–61.
- Allen, J.B., Smith, D.L., 2012. Characterizing the impact of geometric simplification on large woody debris using CFD. *Int. J. Hydrocarb. Eng.* 1, 1–14.
- Alratrout, A., Blunt, M.J., Bijeljic, B., 2018. Wettability in complex porous materials, the mixed-wet state, and its relationship to surface roughness. *Proc. Natl. Acad. Sci. U. S. A.* 115, 8901–8906.
- Amenta, N., Bern, M., 1999. Surface Reconstruction by Voronoi Filtering. *Discrete Comput. Geom.* 22, 481–504.
- Astre, H. 2015. SfMtoolkit, available at: <http://www.visual-experiments.com/demos/sfmtoolkit/>.
- Atha, J.B., Dietrich, J.T., 2016. Detecting Fluvial Wood in Forested Watersheds using LiDAR Data: A Methodological Assessment. *River Res. Appl.* 32, 1587–1596.
- Baillie, B.R., Garrett, L.G., Evanson, A.W., 2008. Spatial distribution and influence of large woody debris in an old-growth forest river system, New Zealand. *For. Ecol. Manag.* 256, 20–27.
- Benda, L.E., Sias, J.C., 2003. A quantitative framework for evaluating the mass balance of in-stream organic debris. *For. Ecol. Manag.* 172, 1–16.
- Benda, L., Miller, D., Sias, J., Martin, D., Bilby, R., Veldhuisen, C., Dunne, T., 2003. Wood recruitment processes and wood budgeting. *Am. Fish. Soc. Symp.* 37, 49–73.
- Berger, M., Tagliasacchi, A., Seversky, L., Alliez, P., Levine, J., Scharf, A., Silva, C., 2014. State of the art in surface reconstruction from point clouds. *Eurographics star reports* 1, 161–185.
- Berger, M., Tagliasacchi, A., Seversky, L., Alliez, P., Guennebaund, G., Levine, J., Scharf, A., Silva, C., 2017. A survey of surface reconstruction from point clouds. *Computer Graphics Forum* 36, 301–329.
- Bilby, R.E., Ward, J.W., 1989. Changes in Characteristics and Function of Woody Debris with increasing size of Streams in Western Washington. *Trans. Am. Fish. Soc.* 118, 368–378.
- Boivin, M. & Buffin-Bélanger, T. 2010. Using a terrestrial lidar for monitoring of large woody debris jams in gravel-bed rivers. *7th Gravelbed Rivers Conference*, 5–10 September 2010, Tadoussac, Quebec, Canada (poster).
- Boivin, M., Buffin-Bélanger, T., Piégay, H., 2015. The raft of the Saint-Jean River, Gaspé (Québec, Canada): A dynamic feature trapping most of the wood transported from the catchment. *Geomorphology* 231, 270–280.
- Boivin, M., Buffin-Bélanger, T., Piégay, H., 2017. Estimation of large wood budgets in a watershed and river corridor at interdecadal to interannual scales in a cold-temperate fluvial system. *Earth Surf. Process. Landf.* 42, 2199–2213.
- Boltcheva, D. & Levy, B. 2016. Simple and scalable surface reconstruction. *[Research Report] LORIA - Université de Lorraine; INRIA Nancy*, hal-01349023v2f, 14.
- Braudrick, C.A., Grant, G.E., 2001. Transport and deposition of large woody debris in streams: a flume experiment. *Geomorphology* 41, 263–283.
- Brown, A., Mcbroom, M., Zhang, Y., 2014. Developing a large woody debris budget for the lower San Antonio River. *Texas Water Development Board* 258.
- Brutto, M., Meli, P., 2012. Computer vision tools for 3D modelling in archaeology. *International Journal of Heritage in the Digital Era* 1 (1), 6.
- Burns, J. H. R. & Delparte, D. 2017. Comparison of Commercial Structure-from-Motion Photogrammetry Software Used for Underwater Three-Dimensional Modeling of Coral Reef Environments. *ISPRS - International Archives of the Photogrammetry, Remote Sensing and Spatial Information Sciences, XLII-2/W3*, 127–131.
- Byrnes, N., Hasbargen, L., 2016. Monitoring channel and woody debris dam configurations in Silver Creek, NY. *Geological Society of America* 48 (2).
- Cave, M., Davies, N., Langford, J., 2017. Cyclone cook slash investigation 2017 report. *Gisborne District Council - Land and Soil Environmental Services and Protection* 121.
- Cazals, F., Giesen, J., 2006. Delaunay Triangulation Based Surface Reconstruction. *Springer, In Effective Computational Geometry for Curves and Surfaces*.
- CGAL 2018. Computational Geometry Algorithms Library. *Online Webpage*: "www.cgal.org".
- Cheng, S. & Lau, M. K. 2017. Denoising a point cloud for surface reconstruction. *arXiv preprint arXiv:1704.04038*.
- Cignoni, P., Callieri, M., Corsini, M., Dellepiane, M., Ganovelli, F. & Ranzuglia, G. 2008. MeshLab: an open-source mesh processing tool. *Proceedings of the 2008 Eurographics Italian Chapter Conference*.
- CLOUDCOMPARE, 2018. Compute 2.5D volume; Description of the computation algorithm. *CloudCompare Wiki Homepage*. http://www.cloudcompare.org/doc/wiki/index.php?title=2.5D_Volume.
- CLOUDCOMPARE 2.5D, 2016. Computation of Mesh\Delaunay 2.5D (XY plane). *CloudCompare Wiki Homepage*. [https://www.cloudcompare.org/doc/wiki/index.php?title=Mesh%5CDelaunay_2.5D_\(XY_plane\)](https://www.cloudcompare.org/doc/wiki/index.php?title=Mesh%5CDelaunay_2.5D_(XY_plane)).
- CLOUDCOMPAREV2 2016 CloudCompare V2, Version 2.6.3, Windows 64-bits.
- Colvard, J. R. 1998. Jamming in Yellowstone: Mapping Lagre Woody Debris in America's first National Park. *Master's Thesis on the Graduate School-NEw Brunswick Rutgers, The State University of New Jersey*, 60.

- Comiti, F., Lucía, A., Rickenmann, D., 2016. Large wood recruitment and transport during large floods: A review. *Geomorphology* 269, 23–39.
- Cordova, J.M., Rosi-Marshall, E.J., Yamamoto, A.M., Lamberti, G.A., 2006. Quantity, controls and functions of large woody debris in Midwestern USA streams. *River Res. Appl.* 13.
- Daniels, M.D., 2006. Distribution and dynamics of large woody debris and organic matter in a low-energy meandering stream. *Geomorphology* 77, 286–298.
- Dassot, M., Colin, A., Santennoise, P., Fournier, M., Constant, T., 2012. Terrestrial laser scanning for measuring the solid wood volume, including branches, of adult standing trees in the forest environment. *Comput. Electron. Agric.* 89, 86–93.
- DELFT3D 2011. Delft3D - Modelling software for simulation of hydrodynamics, sediment transport, morphology and water quality; <https://oss.deltares.nl/web/delft3d/>.
- Dietrich, J.T., 2016. Riverscape mapping with helicopter-based Structure-from-Motion photogrammetry. *Geomorphology* 252, 144–157.
- Dikovski, B., Lameski, P., Zdravski, E. & Kulakov, A. 2014. Structure from motion obtained from low quality images in indoor environment. *Conference Paper - Vitola, Macedonia*, 4.
- Dixon, S.J., Sear, D.A., 2014. The influence of geomorphology on large wood dynamics in a low gradient headwater stream. *Water Resour. Res.* 50, 9194–9210.
- Doneus, M., Verhoeven, G., Fera, M., Briese, C., Kucera, M., Neubauer, W., 2011. From deposit to point cloud - A study of low-cost computer vision approaches for the straightforward documentation of archaeological excavations. *Geoinformatics CTU FCE* 6, 81–88.
- Eltner, A., Kaiser, A., Castillo, C., Rock, G., Neugirg, F., Abellan, A., 2016. Image-based surface reconstruction in geomorphology – merits, limits and developments. *Earth Surface Dynamics* 4, 359–389.
- Fausch, K.D., Northcote, T.G., 1992. Large Woody Debris and Salmonid Habitat in a Small Coastal British Columbia Stream. *Can. J. Fish. Aquat. Sci.* 49, 682–693.
- Ferreira, E., Chandler, J., Wackrow, J., Shiono, K., 2017. Automated extraction of free surface topography using SfM-MVS photogrammetry. *Flow Meas. Instrum.* 54, 243–249.
- Frank, T., Tertois, A.-L., Mallet, J.-L., 2007. 3D-reconstruction of complex geological interfaces from irregularly distributed and noisy point cloud data. *Comput. Geosci.* 33, 932–943.
- Fuchs, H., Kedem, Z.M., Uselton, S.P., 1977. Optimal surface reconstruction from planar contours. *Commun. ACM* 20 (10), 693–702.
- Gao, Z., Yu, Z., Holst, M., 2013. Feature-preserving surface mesh smoothing via suboptimal Delaunay triangulation. *Graph Models* 75, 23–38.
- Geerling, G.W., Labrador-García, M., Clevers, J.G.P.W., Ragas, A.M.J., Smits, A.J.M., 2007. Classification of floodplain vegetation by data fusion of spectral (CASI) and LiDAR data. *Int. J. Remote Sens.* 28, 4263–4284.
- Gippel, C., 1995. Environmental Hydraulics of large Woody Debris in Streams and Rivers. *J. Environ. Eng.* 121 (5), 388–395.
- Grigillo, D., Vrečko, A., Mikoš, M., Gvozdanović, T., Anžur, A., Vežočanik, R., Petrovič, D., 2015. Determination of large wood accumulator in steep forested torrent using laser scanning. *Engineering Geology for Society and Territory* 3, 127–130.
- Gruen, A., 2012. Development and status of image matching in photogrammetry. *Photogramm. Rec.* 27 (137), 36–57.
- Gschntzer, T., Gems, B., Mazzorana, B., Aufleger, M., 2017. Towards a robust assessment of bridge clogging processes in flood risk management. *Geomorphology* 279, 128–140.
- Gurnell, A.M., 2013. Wood in fluvial systems. *Shroder, J. (Editor in Chief), Wohl, E. (Ed.), Treatise on Geomorphology*. Academic Press, San Diego, CA 9, 163–188.
- Gurnell, A.M., Piegay, H., Swanson, F.J., Gregory, S.V., 2002. Large wood and fluvial processes. *Freshw. Biol.* 47, 601–619.
- Harmon, M.E., Franklin, J.F., Swanson, F.J., Sollins, P., Gregory, S.V., Lattin, J.D., Anderson, N.H., Cline, S.P., Aumen, N.G., Sedell, J.R., Lienkaemper, G.W., Cromack, K., Cummins, K.W., 1986. Ecology of Coarse Woody Debris in Temperate Ecosystems. *Adv. Ecol. Res.* 15, 133–302.
- Hildreth, E. C., Ando, H., Anderson, R. A. & Treue, S. 1995. Recovering three-dimensional Structure from Motion with Surface Reconstruction. *Vision Res.*, 35/1, 117–137.
- Hosoi, F., Nakai, Y., Omasa, K., 2013. 3-D voxel-based solid modeling of a broad-leaved tree for accurate volume estimation using portable scanning lidar. *ISPRS J. Photogramm. Remote Sens.* 82, 41–48.
- Hübl, J., Kienholz, H., Loipersberger, A., 2002. DOMODIS - documentation of mountain disasters - state of discussion in the European Mountain areas. *Interprevent* 1, 40.
- Immerzeel, W.W., Kraaijenbrink, P.D.A., Shea, J.M., Shrestha, A.B., Pellicciotti, F., Bierkens, M.F.P., De-Jong, S. M., 2014. High-resolution monitoring of Himalayan glacier dynamics using unmanned aerial vehicles. *Remote Sens. Environ.* 150, 93–103.
- Jackson, C. R. & Sturm, C. A. 2002. Woody debris and channel morphology in first- and second-order forested channels in Washington's coast ranges. *Water Resources Research*, 38, 16-1-16-14.
- Janisch, J., 2006. Standard operating procedures for estimating large woody debris loads intersecting headwater channels.pdf. *Washington State Department of Ecology - Environmental Assessment*. Program 1, 10.
- Javernick, L., Brasington, J., Caruso, B., 2014. Modeling the topography of shallow braided rivers using Structure-from-Motion photogrammetry. *Geomorphology* 213, 166–182.
- Jiang, S., Jiang, W., 2017. Efficient structure from motion for oblique UAV images based on maximal spanning tree expansion. *ISPRS J. Photogramm. Remote Sens.* 132, 140–161.
- Jones, H., 2017. Factsheet: Land Cover and why it is Important (LAWA - LandAirWaterAoteroa).
- Kaiser, A., Neugirg, F., Rock, G., Müller, C., Haas, F., Ries, J., Schmidt, J., 2014. Small-scale surface reconstruction and volume calculation of soil erosion in complex Moroccan Gully morphology using structure from motion. *Remote Sens.* 6, 7050–7080.
- Kasprak, A., Magilligan, F.J., Nislow, K.H., Snyder, N.P., 2012. A lidar-derived evaluation of watershed-scale large woody debris sources and recruitment mechanisms: coastal Maine, USA. *River Res. Appl.* 28, 1462–1476.
- Kazhdan, M., Hoppe, H., 2013. Screened poisson surface reconstruction. *ACM Trans. Graph.* 32, 1–13.
- Kazhdan, M., Bolitho, M. & Hoppe, H. 2006. Poisson Surface Reconstruction. *Eurographics Symposium on Geometry Processing*, 10.
- Kim, S. & Li, R. 2006. Complete 3D surface reconstruction from unstructured point cloud. *Journal of Mechanical Science and Technology*, 20.
- Knauss, J. 1995. *Von der oberen zur unteren Isar*, Versuchsanst. für Wasserbau und Wasserwirtschaft, Oskar-v.-Miller-Inst.
- Lai, Y.G., 2016. Quantitative modeling tools for large woody debris and other in-stream structures. *Reclamation - Managing Water in the West* 159.
- Lai, Y.G., Bandrowski, D.J., 2014. Large wood flow hydraulics: a 3D modelling approach. *International Congress on Environmental Modelling and Software Society.* 22, pp. 2163–2171.
- Le Lay, Y. F., Piégay, H. & Moulin, B. 2013. 12.3 wood entrance, deposition, transfer and effects on fluvial forms and processes: problem statements and challenging issues. 20–36.
- Lienkaemper, G.W., Swanson, F.J., 1987. Dynamics of large woody debris in streams in old-growth Douglas-fir forests. *Can. J. For. Res.* 17, 150–156.
- Lisle, T., 1986. Stabilization of a gravel channel by large streamside obstructions and bed-rock bends, Jacoby Creek, northwestern California. *Geol. Soc. Am. Bull.* 97, 999–1011.
- Liu, W., Zhou, X., Zhang, X., Niu, Q., 2014. Three dimensional 3D CAD model lightweight scheme for large scale assembly and simulation. *Int. J. Comput. Integr. Manuf.* 28, 520–533.
- Macvicar, B.J., Piégay, H., Henderson, A., Comiti, F., Oberlin, C., Pecorari, E., 2009. Quantifying the temporal dynamics of wood in large rivers: field trials of wood surveying, dating, tracking, and monitoring techniques. *Earth Surf. Process. Landf.* 34, 2031–2046.
- Magnussen, S., Nord-Larsen, T., Riis-Nielsen, T., 2018. Lidar supported estimators of wood volume and aboveground biomass from the Danish national forest inventory (2012–2016). *Remote Sens. Environ.* 211, 146–153.
- Maiti, A., Chakravarty, D., 2016. Performance analysis of different surface reconstruction algorithms for 3D reconstruction of outdoor objects from their digital images. *Springerplus* 5, 932.
- Mancini, F., Dubbini, M., Gattelli, M., Stecchi, F., Fabbri, S., Gabbianelli, G., 2013. Using Unmanned Aerial Vehicles (UAV) for high-resolution reconstruction of topography: the structure from motion approach on coastal environments. *Remote Sens.* 5, 6880–6898.
- Manners, R.B., Doyle, M.W., 2008. A mechanistic model of woody debris jam evolution and its application to wood-based restoration and management. *River Res. Appl.* 24, 1104–1123.
- Manners, R.B., Doyle, M.W., Small, M.J., 2007. Structure and hydraulics of natural woody debris jams. *Water Resour. Res.* 43.
- Mao, L., Ugalde, F., Iroume, A., Lacy, S.N., 2017. The Effects of replacing Native Forest on the Quantity and Impacts of In-Channel pieces of large Wood in Chilean Streams. *River Res. Appl.* 33, 73–88.
- Marcus, W.A., Gleleiter, C.J., Aspinall, R.J., Boardman, J.W., Crabtree, R.L., 2003. High spatial resolution hyperspectral mapping of in-stream habitats, depths, and woody debris in mountain streams. *Geomorphology* 55, 363–380.
- Martin, D.J., Harden, C.P., Tran, L., Opavlosky, R.T., 2018. Investigating patterns of in-channel wood deposition locations in a low gradient, variably-confined alluvial river system. *Prog. Phys. Geogr.* 42 (2), 139–161.
- Marton, Z.C., Rusu, R.B., Beetz, M., 2009. On fast surface reconstruction methods for large and noisy point clouds. *IEEE International Conference of Robotics and Automation (ICRA)*, pp. 3218–3223.
- Matsuda, K., Ukita, N., 2011. Direct Shape Carving - Smooth 3D Points and Normals for Surface Reconstruction. *IAPR Conference on Machine Vision Applications in Nara, Japan*, pp. 104–107.
- Mattingly, W.A., Chariker, J.H., Paris, R., Chang, D.J., Pani, J.R., 2015. 3D modeling of branching structures for anatomical instruction. *J. Vis. Lang. Comput.* 29, 54–62.
- Mazzorana, B., Fuchs, S., 2010. Fuzzy Formative Scenario Analysis for woody material transport related risks in mountain torrents. *Environ. Model. Softw.* 25, 1208–1224.
- Mckean, J., Tonina, D., Bohn, C., Wright, C.W., 2014. Effects of bathymetric lidar errors on flow properties predicted with a multi-dimensional hydraulic model. *Journal of Geophysical Research: Earth Surface* 119, 644–664.
- Megahan, W.F., Nowlin, R.A., 1976. Sediment storage in channels draining small forested watersheds in the mountains of central Idaho. v. 1976, 245100.
- MFE 2010. River Environment Classification New Zealand - Ministry for the Environment.
- Micheletti, N., Chandeler, J. H. & Lane, S. N. 2015a. Structure from Motion (SfM) Photogrammetry. *British Society of Geomorphology. In Clarke, L.E. and Nield, J.M. (Eds.) Geomorphological Techniques (Online Edition)*, Chap. 2, Sec. 2.2, 12.
- Micheletti, N., Chandler, J.H., Lane, S.N., 2015b. Investigating the geomorphological potential of freely available and accessible structure-from-motion photogrammetry using a smartphone. *Earth Surf. Process. Landf.* 40, 473–486.
- Miknis, M., Davies, R., Plassmann, P., Ware, A., 2016. Efficient Point Cloud pre processing using the Point Cloud library. *International Journal of Image Processing (IJIP)* 10, 63–72.
- Ministry for Primary Industries 2017. Plantation Forestry Erosion Susceptibility Classification - Risk assessment for the National Environmental Standards for Plantation Forestry. *MPI Technical* 2017/47, 163.
- Mitra, N. J. & Nguyen, A. 2003. Estimating surface normals in noisy point cloud data. *Symposium on Computational Geometry*, 1–7.
- Montgomery, D. R., Collins, B. D., Buffington, J. M. & Abbe, T. B. 2003. Geomorphic effects of wood in rivers. *American Fisheries Society Symposium* 28.
- Morgan, J.A., Brogan, D.J., Nelson, P.A., 2016. Application of Structure-from-Motion photogrammetry in laboratory flumes. *Geomorphology* 276, 125–143.
- Mosley, M.P., 1981. The influence of organic debris on channel morphology and bedload transport in a New Zealand forest stream. *Earth Surf. Process. Landf.* 6, 571–579.

- Nakamura, F., Swanson, F.J., 1994. Distribution of coarse woody debris in a mountain stream, western Cascade Range, Oregon. *Can. J. Fish. Aquat. Sci.* 24, 9.
- Nocerino, E., Lago, F., Morabito, D.R., F., PORZI, L., POIESI, F., Rota Bulo, S., Chippendale, P., Locher, A., Havlena, M., Van Gool, L., Eder, M., Foetschl, A., Hilsmann, A., Kausch, L. & Van Gool, L. 2017. A smartphone-based 3D pipeline for the creative industry - the replicate eu project -. 3D VIRTUAL RECONSTRUCTION AND VISUALIZATION OF COMPLEX ARCHITECTURES, 42 (W3), 535-541.
- Orru, C., Blom, A., Chavarrias, V., Ferrara, V., Stecca, G., 2016. A new technique for measuring the bed surface texture during flow and application to a degradational sand-gravel laboratory experiment. *Water Resour. Res.* 52, 7005-7022.
- Pagliara, S., Carnacina, I., 2010. Temporal scour evolution at bridge piers: effect of wood debris roughness and porosity. *J. Hydraul. Res.* 48, 3-13.
- Palagyi, K., Tschirren, J., Hoffman, E.A., Sonka, M., 2006. Quantitative analysis of pulmonary airway tree structures. *Comput. Biol. Med.* 36, 974-996.
- Pauly, M., Gross, M. & Kobbelt, L. P. 2002. Efficient simplification of point-sampled surfaces. *Proceedings of the conference on Visualization'02 - IEEE Computer Society*, 163-170.
- Peterson, E.B., Klein, M., Stewart, R.L., 2015. Whitepaper on Structure from Motion (SfM) photogrammetry: constructing three dimensional models from photography. *Reclamation - Managing Water in the West* 47.
- Phillips, C., Marden, M., Basher, L.R., 2018. Geomorphology and forest management in New Zealand's erodible steepplands: An overview. *Geomorphology* 307, 107-121.
- Piegay, H., 1993. Nature mass and preferential sites of coarse woody debris deposition in the lower Ain valley (Molton Reach), France. *Regul. Rivers Res. Manag.* 8, 359-372.
- Pix4D Switzerland 2018. Pix4Dmapper pro - Educational, Version 4.1.25.
- PIX4DMAPPER 2018. Pix4Dmapper 4.1 - User Manual. 305.
- PIX4DONLINE 2018. Pix4Dmapper volume calculation - Pix4D Support - Online Website.
- Platts, W. S., Megahan, W. F. & Minshall, G. W. 1983. Methods for evaluating Stream, Riparian, and Biotic Conditions. *United States Department of Agriculture - General Technical Report INT-138, Forest Service*, 76.
- Prosdociuni, M., Calligaro, S., Sofia, G., Fontana, G.D., Tarolli, P., 2015. Bank erosion in agricultural drainage networks: new challenges from structure-from-motion photogrammetry for post-event analysis. *ESPL* 40, 1891-1906.
- Ravazzolo, D., Mao, L., Picco, L., Lenzi, M.A., 2015. Tracking log displacement during floods in the Tagliamento River using RFID and GPS tracker devices. *Geomorphology* 228, 226-233.
- Reddy, P., 2017. Resource management national environmental standards for plantation forestry regulations 2017. New Zealand Legislation - Parliamentary Counsel Office, Ministry for Primary Industries 174, 74.
- Richardson, J.J., Moskal, L.M., 2016. An integrated approach for monitoring contemporary and recruitable large woody debris. *Remote Sens.* 8, 13.
- Rigon, E., Comiti, F., Mao, L., Lenzi, M.A., 2008. Relationships among basin area, sediment transport mechanisms and wood storage in mountain basins of the Dolomites (Italian Alps). *Monitoring, Simulation, Prevention and Remediation of Dense Debris Flows II* 60, 163-172.
- Riley, P., Crowe, P., 2006. Airborne and terrestrial laser scanning - applications for Illawarra coal. *Coal Operators' Conference* 266-275.
- Rosell, J., Llorens, J., Sanz, R., Arno, J., Ribes-Dasi, M., Masip, J., Escola, A., Camp, F., Solanelles, F., Gracia, F., Gil, E., Val, L., Planas, S., Palacin, J., 2009. Obtaining the three-dimensional structure of tree orchards from remote 2D terrestrial LIDAR scanning. *Agricultural and Forest Meteorology* 149, 1505-1515.
- Ruiz-Villanueva, V., Bladé, E., Sánchez-Juny, M., Martí-Cardona, B., Díez-Herrero, A., Bodoque, J.M., 2014a. Two-dimensional numerical modeling of wood transport. *J. Hydroinf.* 16, 1077-1096.
- Ruiz-Villanueva, V., Díez-Herrero, A., Ballesteros, J.A., Bodoque, J.M., 2014b. Potential large woody debris recruitment due to landslides, bank erosion and floods in mountain basins: a quantitative estimation approach. *River Res. Appl.* 30, 81-97.
- Ruiz-Villanueva, V., Piegay, H., Gurnell, A.A., Marston, R.A., Stoffel, M., 2016. Recent advances quantifying the large wood dynamics in river basins: new methods and remaining challenges. *Rev. Geophys.* 54, 611-652.
- Ruiz-Villanueva, V., Mazzorana, B., Bladé, E., Bürkli, L., Iribarren-Anacona, P., Mao, L., Nakamura, F., Ravazzolo, D., Rickenmann, D., Sanz-Ramos, M., Stoffel, M., Wohl, E., 2019. Characterization of wood-laden flows in rivers. *Earth Surf. Process. Landf.* 44, 1694-1709.
- Rusu, R. B. 2009. Semantic 3D object maps for everyday manipulation in human living environments - Dissertation. 284.
- Rusu, R.B., Cousins, S., 2011. 3D is here: Point Cloud Library (PCL). *Robotics and Automation (ICRA)*, 2011 IEEE International Conference, pp. 1-4.
- Rusyd, M.I., Hashimoto, H., Ikematsu, S., 2014. Log jam formation by an obstruction in a river. *River Flow* 2014, 717-724.
- Sanhueza, D., Iroumé, A., Ulloa, H., Picco, L. & Ruiz-Villanueva, V. 2018. Measurement and quantification of fluvial wood deposits using UAVs and structure from motion in the Blanco River (Chile). *5th IAHR Europe Congress - New Challenges in Hydraulic Research and Engineering, Proc. of the 5th IAHR Europe Congress*.
- Sanhueza, D., Zingaretti, V., Iroumé, A. & Picco, L. 2019. Using UAV and structure from motion to study large wood dynamics in a highly disturbed reach of the Blanco-Este river (Calbuco, Chile). *Proceedings of the 4th International Conference Wood in World Rivers*.
- Schalko, I., Schmockler, L., Weitbrecht, V., Boes, R., 2016. Modeling the effect of organic fine material in a driftwood accumulation on backwater rise. *River Flow* 2016, 2326-2332.
- Schalko, I., Schmockler, L., Weitbrecht, V., Boes, R.M., 2018. Backwater rise due to large wood accumulations. *J. Hydraul. Eng.* 144, 04018056.
- Schalko, I., Lageder, C., Schmockler, L., Weitbrecht, V., Boes, R.M., 2019. Laboratory flume experiments on the formation of spanwise large wood accumulations part I: effect on backwater rise. *Water Resour. Res.* 55, 4854-4870.
- Schenk, E.R., Moulin, B., Hupp, C.R., Richter, J.M., 2014. Large wood budget and transport dynamics on a large river using radio telemetry. *Earth Surf. Process. Landf.* 39, 487-498.
- Schmockler, L., Weitbrecht, V., 2013. Driftwood: risk analysis and engineering measures. *J. Hydraul. Eng.* 139, 683-695.
- Seitz, L., Haas, C., Noack, M., Wieprecht, S., 2018. From picture to porosity of river bed material using Structure-from-Motion with Multi-View-Stereo. *Geomorphology* 306, 80-89.
- Shepherd, P. & Treddinick, J. 2015. Rapid processing of 3D colour point clouds for 3D printing. *Proceedings of International Association for Shell and Spatial Structures (IASS)*, 10.
- Shields, F.D., 2001. Effect of Large Woody Debris Structures on Stream Hydraulics. From Proceedings of the conference on Wetland Engineering and River Restoration, Reno, Nevada, pp. 27-31.
- Skagit Watershed Council, 2017. Skagit River Large Woody Debris Assessment - Skagit Watershed Council. *Natural Systems Design* 36.
- Smith, M.W., Vericat, D., 2015. From experimental plots to experimental landscapes: topography, erosion and deposition in sub-humid badlands from Structure-from-Motion photogrammetry. *Earth Surf. Process. Landf.* 40, 1656-1671.
- Smith, D.L., Allen, J.B., Eslinger, O., Valenciano, M., Nestler, J., Goodwin, R.A., 2011. Hydraulic modeling of large roughness elements with computational fluid dynamics for improved realism in stream reconstruction planning. *Stream Restoration in Dynamic Fluvial Systems: Scientific Approaches, Analyses, and Tools*. Geophysical Monograph Series 194, 115-123.
- Smith, M.W., Carrivick, J.L., Quincey, D.J., 2016. Structure from motion photogrammetry in physical geography. *Prog. Phys. Geogr.* 40 (2), 247-275.
- Snapir, B., Hobbs, S., Waine, T.W., 2014. Roughness measurement over an agricultural soil surface with Structure from Motion. *ISPRS - International Archives of the Photogrammetry and Remote Sensing* 96, 210-223.
- Steeb, N., Rickenmann, D., Badoux, A., Rickli, C., Waldner, P., 2017. Large wood recruitment processes and transported volumes in Swiss mountain streams during the extreme flood of August 2005. *Geomorphology* 279, 112-127.
- Swanson, F.J., Lienkaemper, G.W., Sedell, J.R., 1976. History, Physical Effects, and Management Implications of Large Organic Debris in Western Oregon Streams *USDA Forest Service General Technical Report PNW-56*, 21.
- Tazir, M., Checchin, P., Trassoudaine, L., 2016. Color-based 3D point cloud reduction. 14th International Conference on Control, Automation, Robotics and Vision (ICARCV)-IEEE, p. 7.
- Thevenet, A., Citterio, A., Piegay, H., 1998. A new methodology for the assessment of large woody debris accumulations on highly modified rivers. *Regulated Rivers: Research & Management* 14, 467-483.
- Tonon, A., Picco, L., Ravazzolo, D., Lenzi, M.A., 2014. Using a terrestrial laser scanner to detect wood characteristics in gravel-bed rivers. *Journal of Agricultural Engineering* 45, 161.
- Tonon, A., Iroumé, A., Picco, L., Oss-Cazzador, D., Lenzi, M.A., 2017. Temporal variations of large wood abundance and mobility in the Blanco River affected by the Chaitén volcanic eruption, southern Chile. *Catena* 156, 149-160.
- Tonon, A., Picco, L., Rainato, R., 2018. Test of methodology for developing a large wood budget: A 1-year example from a regulated gravel bed river following ordinary floods. *Catena* 165, 115-124.
- TRRP 2018. Trinity River Restoration Program. *Online Webpage: "http://www.trrp.net/"*.
- Truksa, T., Bowman, J., Goode, J., 2017. Can drones measure LWD?: high resolution aerial imagery and structure from motion as a method for quantifying instream wood. *Geological Society of America* 49 (6).
- Tunncliffe, J., Brierley, G., Fuller, I.C., Leenan, A., Marden, M., Peacock, D., 2018. Reaction and relaxation in a coarse-grained fluvial system following catchment-wide disturbance. *Geomorphology* 307, 50-64.
- Uchiogi, T., Shima, J., Tajima, H. & Ishikawa, Y. 1996. Design methods for wood-debris-entrapment. *Proceedings of the Interpvent Conference*, 5, 279-288.
- Ulloa, H., Iroumé, A., Mao, L., Andreoli, A., Díez, S., Lara, L.E., 2016. Use of remote imagery to analyse changes in morphology and longitudinal large wood distribution in the Blanco river after the 2008 chaitén volcanic eruption, southern Chile. *Geografiska Annaler: Series A, Physical Geography* 97, 523-541.
- Ventres-Pake, R., Nahorniak, M., Kramer, N., O'Neill, J., Abbe, T., 2019. Integrating large wood jams into hydraulic models: evaluating a porous plate modeling method. 4th International Conference on Wood in World Rivers 2019, Chile, Valdivia.
- Verbree, E., Van Oosterom, P., 2003. THE STIN METHOD: 3D-SURFACE RECONSTRUCTION BY OBSERVATION LINES AND DELAUNAY TENS *Commission III. WG 3*, 6.
- VISUALSFM 2018. VisualSFM Online platform, available at: <http://ccwu.me/vsfm/>.
- Wallace, L., Lucier, A., Malenovsky, Z., Turner, D., Vopenka, P., 2016. Assessment of forest structure using two UAV techniques - a comparison of airborne laser scanning and structure from motion (SfM) point clouds. *Forests* 7 (62), 16.
- Webb, A.A., Erskine, W.D., 2003. Distribution, recruitment, and geomorphic significance of large woody debris in an alluvial forest stream: Tonghi Creek, southeastern Australia. *Geomorphology* 51, 109-126.
- Westoby, M.J., Brasington, J., Glasser, N.F., Hambrey, M.J., Reynolds, J.M., 2012. 'Structure-from-Motion' photogrammetry: a low-cost, effective tool for geoscience applications. *Geomorphology* 179, 300-314.
- Wohl, E., Jaeger, K., 2009. A conceptual model for the longitudinal distribution of wood in mountain streams. *Earth Surf. Process. Landf.* 34, 329-344.
- Wohl, E., Scott, D.N., 2017. Wood and sediment storage and dynamics in river corridors. *Earth Surf. Process. Landf.* 42, 5-23.
- Wohl, E., Lininger, K.B., Fox, M., Baillie, B.R., Erskine, W.D., 2017. Instream large wood loads across bioclimatic regions. *For. Ecol. Manag.* 404, 370-380.
- Wright, A., Marcus, W.A., Aspinall, R., 2000. Evaluation of multispectral, fine scale digital imagery as a tool for mapping stream morphology. *Geomorphology* 33, 107-120.

- Wróżyński, R., Pyszny, K., Sojka, M., Przybyła, C., Murat-Błażejewska, S., 2017. Ground volume assessment using 'Structure from Motion' photogrammetry with a smartphone and a compact camera. *Open Geosciences* 9.
- Wu, C., 2013. Towards linear-time incremental structure from motion. *International Conference on 3-D Vision - 3-DV*, Seattle, WA, USA, pp. 127–134.
- Wu, J., Kobbelt, L., 2004. Optimized sub-sampling of point sets for surface splatting. *Eurographics 2004* (23), 10.
- Xu, Y., Liu, X., 2017. Effects of different in-stream structure representations in computational fluid dynamics models—taking Engineered Log Jams (ELJ) as an example. *Water* 9, 21.
- Yang, L., Hyde, D., Grujic, O., Scheidt, C., Caers, J., 2019. Assessing and visualizing uncertainty of 3D geological surfaces using level sets with stochastic motion. *Comput. Geosci.* 122, 54–67.
- Zhang, R., Schneider, D. & Strauß, B., 2016. Generation and Comparison of Tls and Sfm based 3d Models of Solid Shapes in Hydromechanic Research. *ISPRS - International Archives of the Photogrammetry, Remote Sensing and Spatial Information Sciences*, XLII-B5, 925–929.
- Zhang, Z., Cao, L., She, G., 2017. Estimating forest structural parameters using canopy metrics from airborne LiDAR data in subtropical forests. *Remote Sens.* 9, 26.
- Zischg, A., Galatioto, N., Deplazes, S., Weingartner, R., Mazzorana, B., 2018. Modelling spatiotemporal dynamics of large wood recruitment, transport, and deposition at the river reach scale during extreme floods. *Water* 10, 1134.